POLITECNICO DI TORINO

PHD SCHOOL IN
PHYSICS

PhD Thesis

Tactile sensor devices exploiting the tunnelling conduction in piezoresistive composites

Stefano Stassi

Supervisor
Prof. Candido Fabrizio Pirri

Coordinator of PhD program in Physics
Prof. Arianna Montorsi

XXV cycle: 2010-2012

"The mind that opens to a new idea will never return to its original size."

Albert Einstein

Acknowledgments

First of all I wish to thank my supervisor Professor Fabrizio Pirri for the great opportunity to perform my PhD in his research group in Politecnico di Torino and Center for Space Human Robotics of Istituto Italiano di Tecnologia. He has believed in my capabilities and support the project I developed and I hope to have returned his choice with my work.

Right after, I want to thank Dr.Giancarlo Canavese who helped me to move my first step in the research world and collaborated in the development of the tactile sensor project.

I want to thank all the researcher of CSHR@Polito and Politecnico di Torino for the help to overcome all the obstacles we came across during the project and to reach all the goals. In particular I want to remember Valentina, Andrea, Adriano, Rossana, Nadia, Annalisa, Alberto, Ismael, Diego, Alain and Fai for the friendly environment they have contributed to create in the working place and for the nice time we spent out of work.

I wish to thank all my friends from Cuneo and of the soccer teams for the fun time we had during my free time, helping me to disconnect my mind from the several problems of the project.

Biggest thanks goes to my parents, Gianpiero and Caterina, and my sister Enrica who have supported my dreams once more and provided me with everything I needed in order to achieve my personal goals. I only hope to make them proud of me and to return their generosity.

Finally a special thanks to Margherita who always stayed at my side in the good and bad times supporting me for the whole PhD experience.

Contents

Introduction **2**

1 Tactile sensing **6**

1.1 Human sense of touch 7

1.2 Specific requirements for tactile sensing devices 10

1.3 Classification of tactile sensors 12

1.3.1 Capacitive sensors 13

1.3.2 Optical sensors 16

1.3.3 Piezoelectric sensors 17

1.3.4 Magnetic sensors 19

1.3.5 Ultrasonic sensors 20

1.3.6 Resistive sensors 21

1.3.6.1 Strain gauges 21

1.3.6.2 MEMS piezoresistors 22

1.3.6.3 Piezoresistive polymers and fabrics 23

1.3.6.4 Piezoresistive composite materials 25

2 Theory of piezoresistive effect in composite materials **36**

2.1 Piezoresistive conductor-insulator composites 38

2.1.1 Percolation conduction mechanism 38

2.1.2 Tunnelling conduction mechanism 40

2.1.2.1 Piezoresistivity under compressive pressure 41

2.1.2.2 Piezoresistivity under tensile pressure 44

3 Spiky nanostructured nickel particles as filler of composites showing tunable electrical conductivity 50
3.1 Preparation of the composite . . . 51
3.2 Characterization methods . . . 52
3.3 Structural and morphological analysis . . . 54
3.4 Functional characterization under compressive pressure . . . 55
3.5 Comparison of experimental and simulated piezoresistive response . . . 60
3.6 Mechanical characterizations . . . 62
3.7 Electrical characterization . . . 64
3.8 Electrical and functional response at different temperature . . . 68

4 An innovative PDMS-copper piezoresitive composite for flexible tactile sensor 72
4.1 Preparation of the composite . . . 73
4.2 Structural and morphological analysis . . . 74
4.3 Functional characterization under compressive pressure . . . 74
4.4 Functional characterization under tensile pressure . . . 77

5 Synthesis and integration of spiky nanostructured gold particles as filler of polymeric composites 82
5.1 Experimental Section . . . 84
5.2 Synthesis results . . . 85
5.3 Mathematical model of particles growth . . . 90
5.4 Composite preparation and characterization . . . 92

6 Evaluation of the conductive nanostructured particles as filler in tunnelling piezoresistive composites 96
6.1 Methods of analysis . . . 97
6.2 Comparison between the three piezoresistive composite . . . 98
6.3 Conclusion . . . 102

7 Fabrication of a flexible piezoresistive matrix tactile sensor for humanoid robot 106
7.1 Processability of the composite . . . 108
7.1.1 Technological process flows . . . 108

7.1.2 Material characterization 110
7.2 First generation matrix tactile sensor 113
7.2.1 Sensor design and readout circuitry 113
7.2.2 Device calibration 115
7.2.3 Sensor characterization 117
7.3 Second generation matrix tactile sensor 119

8 A quasi-digital wireless system for piezoresistive composite sensors 124
8.1 Sensor network architecture 124
8.1.1 R,C-to-F converter 126
8.1.2 IC-UWB transmitter 127
8.2 Prototype fabrication 127

Conclusion 132

List of Publications 134

Introduction

During the initial era of automation focused on the industrial robotics, the sensing technology was mainly restricted to joint force/torques, for both safety and operational reasons.

Nowadays the design of humanoid robots for an utilization in complex human environment has created a research focus for the fabrication of devices to sense mechanical strain with the aim to reproduce the human sense of touch. Many different working principles have been exploited to evaluate mechanical pressure: piezoelectric, capacitive and piezoresistivity are the most diffused, but several other exotic approaches have been also reported. However, most of these methods bring to solutions with large pay load, reduced flexibility and thus unsuitable for integration on a robot body.

One of the most promising strategies to fabricate large area or whole-body tactile sensing structures with a high sensitivity is the development of hybrid systems, due to the possibility of combining the desirable characteristics of the filler and matrix and the great number of possible synergistic properties and functionalities. Ease conformability, tailoring functionalities and cost efficient processes are just some of the advantages that have promoted the research of electrical conductive composite systems as tactile sensors.

In particular piezoresistive composites exploiting tunnelling conduction mechanism are very interesting, because even a small deformation can cause a reduction of the electrical resistance of orders of magnitude. Without any external pressure, the metallic fillers are distributed throughout the elastomeric matrix separated between each other by a layer of polymer, thus the overall composite behaves like an insulator. Upon the application of a mechanical deformation, the insulating interparticle layer decreases, thus increasing the tunneling probability of the electrons between two adjacent particles, as sketched in Fig.1. Moreover the high mechanical flexibility, conferred by the polymer, combined with the tunability from the insulating to conductive electrical behavior, makes this kind of composite the ideal candidate to constitute a smart sensing skin for robotic applications. In particular,

these piezoresistive materials could satisfy the main requirements, such as (i) high conformability and compliance, leading to soft materials adaptable to arbitrary curved surfaces and shapes; (ii) broad range and high sensitivity; (iii) large area coverage; (iv) low power consumption, since the composite behaves like an insulator when no load is applied; (v) low payload; (vi) broad working temperature range, mainly depending on the polymer matrix; and (vii) insensitivity to electromagnetic field noise. Moreover, due to their simple construction, generally these composites are very robust to overpressures, shocks and vibrations.

This thesis presents the development and characterization of three different metal-polymer piezoresistive composites with tunable sensitivity and their integration as functional material into tactile sensors. The tunnelling conduction mechanism ensures variation of electrical resistance up to nine orders of magnitude. Two different sensor design have been fabricated with the synthesized composites, tested and mounted on the robotic assistant EUROBOT designed by Thales ESA (European Space Agency).

The thesis consists of eight chapters. The first two are an overview on the tactile sensors research and of the theoretical conduction models for tunnelling conductive composites, while the next six ones regards the experimental work. Chapter 1 describes the human sense of touch and categorizes the tactile sensor devices presented in literature on the basis of the transduction method. Chapter 2 gives an analysis of the mathematical models to describe the conduction inside piezoresistive composite. Chapters 3, 4 and 5 present the preparation and characterization of the piezoresistive composites fabricated with nickel, copper and gold as filler, respectively. Chapter 6 compared the functional response of the three composites. Chapter 7 and 8 describe the fabrication of two different sensor architectures, the first directly measuring the resistance of each nodes in a sensing matrix, while the second evaluating the frequency shift of an AC voltage signal due to a variation of resistance and capacitance of the composite induced by a mechanical deformation.

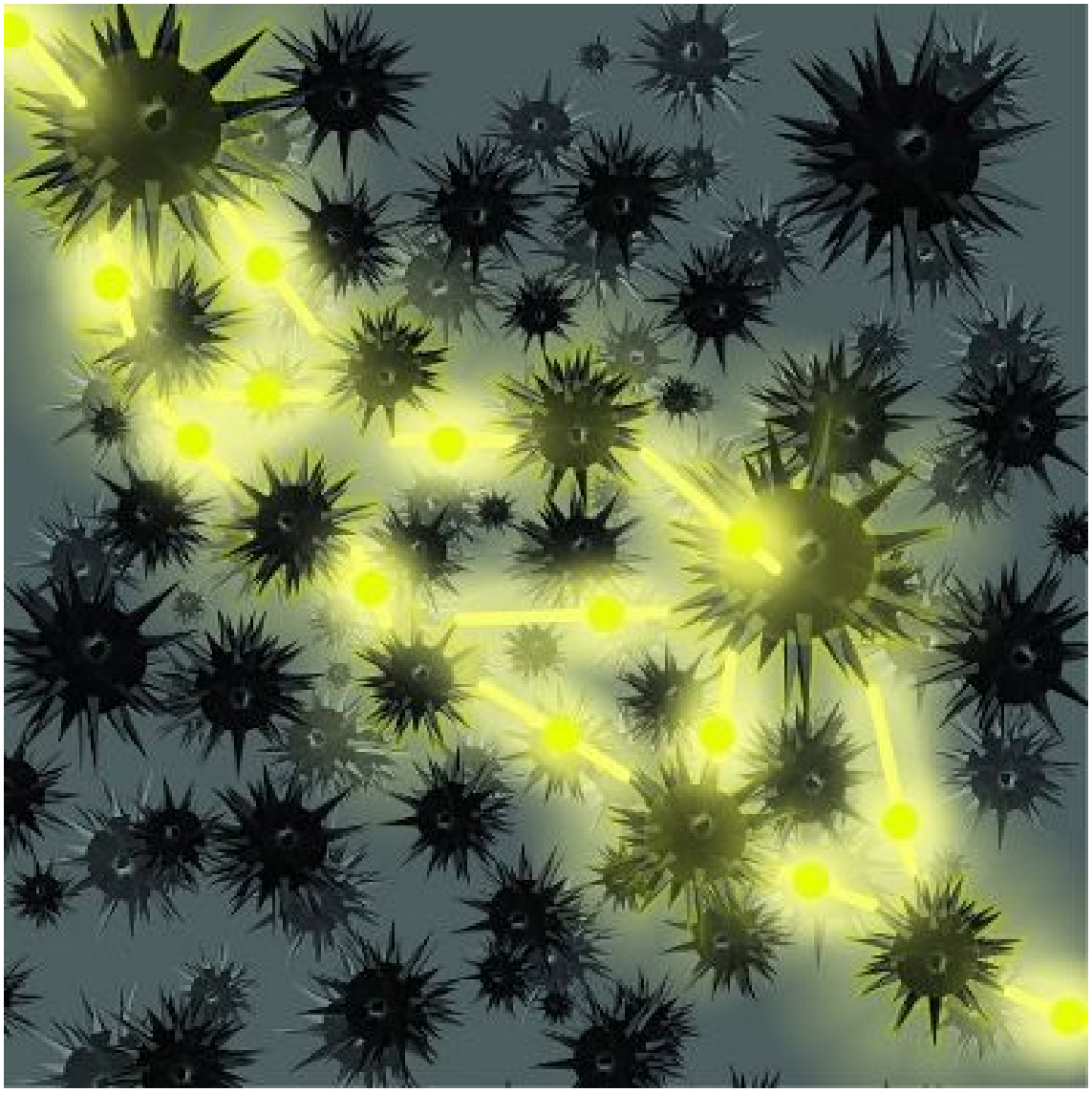

Figure 1. Graphical artwork representing the conduction mechanism in tunnelling piezoresistive composites. The picture appeared on the front cover of the *Journal of Polymer Science: Polymer Physics*, vol_50, N_14 (2012).

Chapter 1

Tactile sensing

The challenge to transfer robots from the confined environment of a production line to complex human environments, where smart tasks and increasingly difficult operations are required, pushes towards the improvement not only of in-hand manipulation and exploration tasks, but also of safe interactions. Humanoid robots, unlike the industrial ones, are required to reach their goals interacting with humans and their tools, adapting to the changes in the environment thanks to an autonomous learning. In order to satisfy these requirements, robots need to be able to perform advanced human-like manipulation tasks such as rotation, translation and in-hand grasping [1].

To operate in changing environments, humanoid robots needs to sense and elaborate the information about the surrounding environment, while interacting with real world objects. Analyzing the force and the position at all points of contact, robots can obtain information about the weight, the stiffness and the surface of the tool and elaborate a way to complete the assigned tasks. In order to satisfy these requirements, there is an increased interest in the robotic community for the development of large area or whole-body tactile sensing structures. Without a performing tactile sensing system, humanoid projects strongly limit their interaction and cognitive capabilities [2]. Also in human, tactile sensing is essential for fine manipulation tasks. In winter or after touching ice blocks our hands are chilled, simple operations like lacing up the shoes or simply maintaining a stable grasp on an object can become very complex tasks. The problem is a lost of sensing, in fact, our mechanoreceptors are anesthetized and our movements become inaccurate and clumsy.

In the last twenty years, many tactile sensor solutions have been presented, exploiting several physical phenomena as transduction modes [1, 2, 3]. However, most of them do not

satisfy completely the specific requirements of in-hand manipulation, being to bulky to be used without sacrificing dexterity or because they are fragile, rigid, slow or lack fundamental characteristics. For this reason, it is not possible to choose a standard system like CCD or CMOS optical arrays for sight sense. Moreover tactile sensors get the informations through physical interaction, this brings problem of robustness, to withstand several impacts and abrasions, and of compliance, to conform the device to the robot surface guaranteeing an adequate friction for handling tools securely [3].

A successful way to design a tactile sensor satisfying the above requirements is to get inspiration from the study of the human skin and sense of touch. Along human history, engineers have always been inspired by biological systems, for example to project airplane from birds and hook-and-loop fastener (better know as Velcro®) from the burrs of burdock, and as well now roboticists are inspired by the human physiology [4, 5]. Such analysis would help in defining the specific requirements (like force resolution, working range, location, and robustness) and in designing robots more suitable for working in a human environment. For this reason this chapter will firstly present a description of the human sense of touch, with the definition of the specific requirements for the design of a tactile sensing structures and then a review of the main classes of sensors with a special consideration on the piezoresistive ones.

1.1 Human sense of touch

The sense of touch in humans is divided in two main modalities, depending on the site of sensory inputs. The kinesthetic sense receives the inputs from the receptors within muscles, tendons, and joints, while the cutaneous from the receptors embedded in the skin [6, 7]. The receptors are not limited to detect the mechanical stimulations, but are also sensitive to the temperature variation and various stimuli producing pain.

The kinesthetic system gives information about the static and dynamic body postures (relative positioning of the head, torso, limbs, and end effectors) on the basis of sensing from the muscles, joints, and tendons and from efference copy, which is the correlate of muscle efference available to the higher brain. On the contrary, the cutaneous system involves physical contact with the stimulus and provides awareness of the stimulation of the outer surface of body by means of receptors in the skin and associated somatosensory area of central nervous system (CNS) [6, 8]. Moreover, the sensing elements of the cutaneous sensing work

not only as transducers, as the kinesthetic ones, but studies showed that they locally process the stimulus before sending tactile data to the somatosensory cortex of CNS for perceptual interpretation [9]. The trasmission of the electrical signal between the receptors have been found to be pyroelectric and piezoelectric [10]. The perception of the external stimuli is done by a large number of receptors (e.g., mechanoreceptors for pressure, thermoreceptors for temperature, and nocioceptors for pain [11]) that are distributed all over the skin with variable density. The mechanoreceptive afferent neurons (mechanoreceptors) represent for the human a distribution of force/pressure/stress sensors over the whole skin. For this tasks they are the biological analogy we would like to reproduce with the piezoresistive composites in this thesis work.

The mechanoreceptors, embedded in the skin at different depths, are divided in four different types depending on their function, sensing ranges and rates of adaption as summarized in Fig.1.1. Fast-adapting afferents respond to temporal changes in skin deformations (dynamic) with burst of action potentials when the stimulus is applied or removed. In contrast slow-adapting afferents respond to sustained pressure over time (static). Both families are divided in two types depending on their location in the depth of the skin and their receptive field. Type I receptors are located in the dermal-epidermal boundary and have small and well-defined receptive fields, while the type II are found in deeper layers of the skin and have larger and more diffuse receptive fields [1, 2, 12].

Under the application of a stimulus, the skin conforms its surface projecting the deformation to a large number of mechanoreceptors. If the magnitude of the stimulus is above the threshold, each receptor (representing a part of interesting area) encodes the tactile information generating a spikes of action potentials-voltage pulses. The amplitude of the stimulus is then converted to a train of action potentials in a process similar to the digitalization of an analog signal in electronics [13]. Then the signal is transmitted to the brain for higher level processing and interpretation via multiple nerves up to the spinal cord and via two major pathways: spinothalamic and dorsal-column-medial-lemniscal (DCML), as shown in Fig.1.1. The spinothalamic pathway is slower and carries temperature and pain-related information, while DCML quickly transfer mechanical related information to the central nervous system. To reduce the amount of data towards the CNS and speed up the spatio-temporal perception of the stimulus, the tactile information are selected and processed at various transfer stages [2].

The limitation and sensitivity of the receptors affect the recognition of the shape of

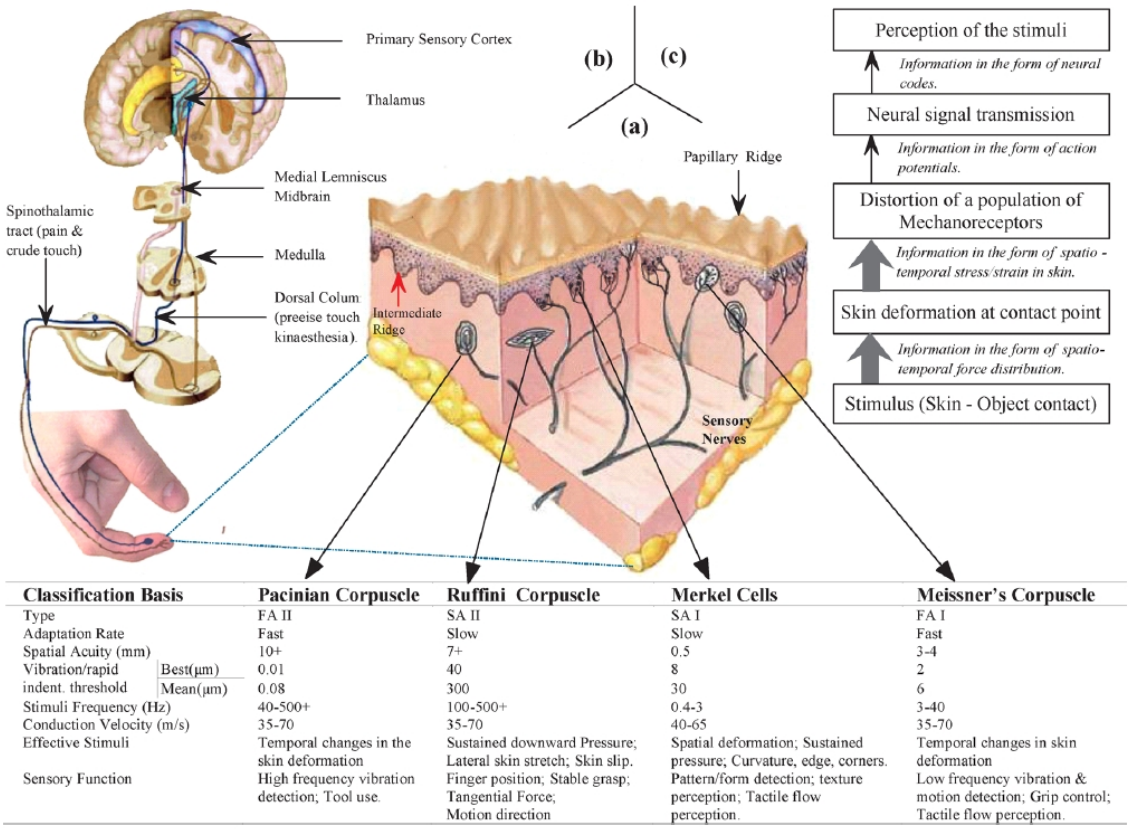

Classification Basis		Pacinian Corpuscle	Ruffini Corpuscle	Merkel Cells	Meissner's Corpuscle
Type		FA II	SA II	SA I	FA I
Adaptation Rate		Fast	Slow	Slow	Fast
Spatial Acuity (mm)		10+	7+	0.5	3-4
Vibration/rapid indent. threshold	Best(μm)	0.01	40	8	2
	Mean(μm)	0.08	300	30	6
Stimuli Frequency (Hz)		40-500+	100-500+	0.4-3	3-40
Conduction Velocity (m/s)		35-70	35-70	40-65	35-70
Effective Stimuli		Temporal changes in the skin deformation	Sustained downward Pressure; Lateral skin stretch; Skin slip.	Spatial deformation; Sustained pressure; Curvature, edge, corners.	Temporal changes in skin deformation
Sensory Function		High frequency vibration detection; Tool use.	Finger position; Stable grasp; Tangential Force; Motion direction	Pattern/form detection; texture perception; Tactile flow perception.	Low frequency vibration & motion detection; Grip control; Tactile flow perception.

Figure 1.1. (a) Section of skin showing the location and classification of the various mechanoreceptors, (b) dynamics of the tactile signal transmission from the sensing area on the fingertip up to the somatosensory area of the central nervous system and (c) events during tactile signal transmission from the stimulus to the brain [2].

objects and of the direction and magnitude of the force. Focusing on the hands type I mechanoreceptors are more concentrated in the fingertips and decrease proximally towards the palm, while the density of the type II is more uniform throughout the whole hand. Moreover there is a predominance of fast adapting type I receptors in the hand indicating the importance of high spatial and temporal resolution in dynamic mechanical interactions, like creation and variation of contact with the object. The spacial concentration of the different mechanoreceptive afferent neurons is shown in Fig.1.2. These two points suggest that the fingertips and phalanges are mainly responsible for movements for direct manipulation of objects, and that the signals coming from the whole hand, hence with a lower temporal and spatial resolution, are important for maintaining stability during manipulation. Talking

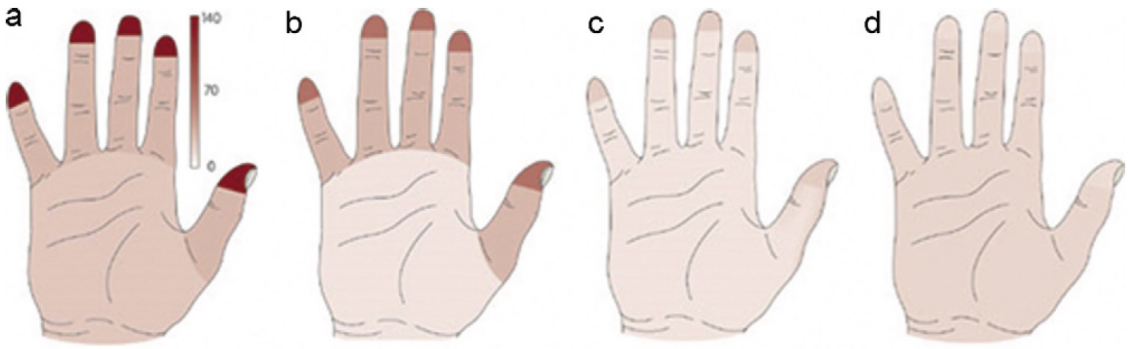

Figure 1.2. Mechanoreceptors density (afferents per cm^2) in the human hand. (a) Fast-adapting type I (FA I), (b) slow-adapting type I (SA I), (c) fast-adapting type II (FA II) and (d) slow-adapting type II (SA II). The scale bar for the colour coding is presented in (a) [1].

about spatial resolution, a person can distinguish two different points of contact as close as 1 mm on the fingertips. This resolution decreases in the other parts of the body up to reach the lowest value (30 mm) in the belly [14].

For what concerns temporal resolution, humans can detect dynamic signal on the same contacty point with a frequency up to 700 Hz (minimum time distance between two noticeable signal of 1.4 ms) [8]. Otherwise the critical temporal separation for two contact events at different locations is around 30-50 ms. All these values are referred to the fingertips that are the most sensitive part, while the time intervals expanded for the rest of the body.

Another parameter involved in determining the tactile sensitivity of the skin is the pressure threshold to activate the mechanoreceptors. The higher the pressure threshold, the lower the sensitivity of the body part. It is interesting to notice that the pressure threshold is much different between men and women. The first have average values of about 0.158 g on the palm and about 0.055 g on the fingertips, while the latter 0.032 g and 0.019 g, respectively [15].

1.2 Specific requirements for tactile sensing devices

On the basis of the consideration brought out during the study of the human sense of touch, some functional requirements can be defined as basic design criteria for the fabrication of a robotic tactile sensor system. The following points are an elaboration of the hints found in [1, 2, 16] and they are summarized in Tab.1.1.

- The device has to be able to detect both static and dynamic contact, distinguish release, lift and replacement of an object.

- The spacial resolution of the sensing arrays should be based on the robot body sites. It has to be at least 1 mm in the fingertips, while it can be lower in less sensitive part like palm, limbs and belly.

- The robots has to appreciate the direction of the force, thus measuring the normal and the tangential components.

- Tactile sensors need a high sensitivity and a wide working range. A force sensitivity range of 0.01 N -10 N is desirable, even if variation could be made depending on the application.

- Faster response of the order of 1 ms are needed, in particular in robots where tactile information are used as control feedback. Less performing device could be used on limbs or other body parts.

- The sensor has to be stable, repeatable, as much as possible linear and without hysteresis phenomena. While nonlinearity can be canceled out with an inverse compensation circuit, taking care of the hysteresis is a more challenging task.

- The robotic sensible area should be flexible, soft, and stretchable in order to conform to the object shape. Therefore, it should withstand mechanical impacts and abrasions, harsh conditions of temperature, humidity, chemical stresses, electric field, sudden force, etc. Moreover when integrated over the body, it should not be too bulky, since significantly increasing of the dimension of robot part worsen the motion performance.

These design criteria are almost exhaustive, but should not be considered definitive. Moreover they could be modified depending on the specific application in which the robot will be used. Even if some criteria are strict and technologically challenging, a possible solution to fulfill them are complex systems integrating different devices instead of using a single tactile sensor.

Parameter	Requirements
Force direction	Both normal and tangential
Temporal variation	Both static and dynamic
Spatial resolution	1 mm on fingertips, 5 mm on the palm, even less elsewhere
Time resolution	1 ms
Force sensitivity	0.01 N - 10 N (1000:1)
Linearity/hysteresis	Stable, repeatable and low hysteresis
Robustness	Depending on the application and environment
Shielding	Electronic and magnetic shielding
Integration and fabrication	Simple and not bulky mechanical integration, minimal wiring, low power consumption and cost

Table 1.1. Specific requirements for the design of a tactile sensor device inspired by the physiology of the human skin [1].

1.3 Classification of tactile sensors

The solutions presented in literature for the fabrication of a tactile sensors are innumerable, so that a deep classification based on task, site, transduction method and mechanical properties (as shown in Fig.1.3) is necessary to organize and select the interested field [2, 17].

Considering the working task, they can be divided in two categories: (i) "Perception for Action", as in grasp control and dexterous manipulation, and "Action for Perception", as in exploration, recognition and evaluation of mechanical properties of the object [2].

Depending on the location of a sensor on a robot body, the sensing capability can be classified as extrinsic and intrinsic sensing. Intrinsic sensors, aimed at the replication of the kinesthetic sensing in humans, are usually placed within the mechanical structure of the system and collect data such as magnitude of force and torque [18]. Extrinsic or tactile sensors/sensing arrays are mounted at the contact interface and, similarly to the cutaneous sensing, they collect data from localized regions [19, 20]. Extrinsic tactile sensors can further be divided depending on the resolution they can achieve. High density tactile sensing arrays are designed for highly sensitive area like fingertips and have to satisfy the requirements of 1 mm and few milliseconds of spatial and temporal resolution respectively. On the contrary, in the large area tactile sensing devices the spatio-temporal constraints can be relaxed since they are designed for less sensitive part as palm, limbs and body.

On the basis of the mechanical properties, the tactile sensors can be labeled as rigid,

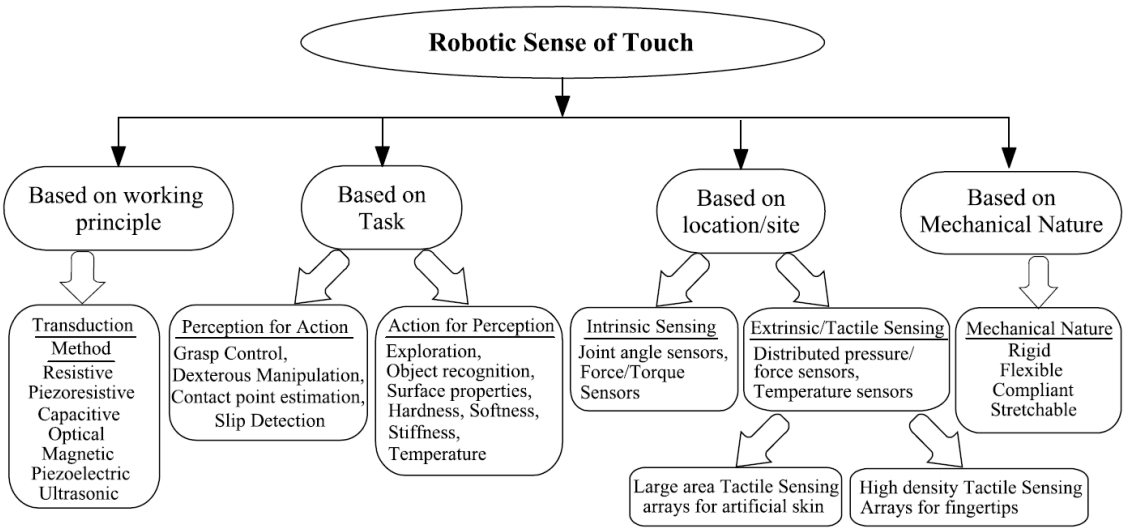

Figure 1.3. Classification of tactile sensing in robotics based on transduction methods, task, site and mechanical properties [17].

flexible, compliant, conformable, stretchable, etc.

The last classification is made with regard to the physical nature of the transduction method. The tactile devices can be divided in resistive (piezoresistive), capacitive, optical, magnetic, piezoelectric and ultrasonic. In the following sections will be presented a brief description of the physical principle involved, of the more representative examples and a list of advantages and disadvantages, with a special focus on the device of the piezoresistive family, which are the sensors developed in this thesis work.

1.3.1 Capacitive sensors

Capacitive principle is the transducer method that guarantees one of the highest sensitivity and besides is temperature independent [22]. The devices measure the capacitance variation due to the coupling with the human capacitance or, in the case of objects, to the deformation of the dielectric layer. Classical capacitive sensors are constituted by an array of capacitive nodes consisting in two parallel metal electrodes divided by a flexible insulating material. The simplicity of the structure allowed capacitive sensors to become widely diffused among tactile devices. Arrays of capacitor elements have been widely fabricated with micro-electro-mechanical-technology (MEMS) and Si micromachining technology

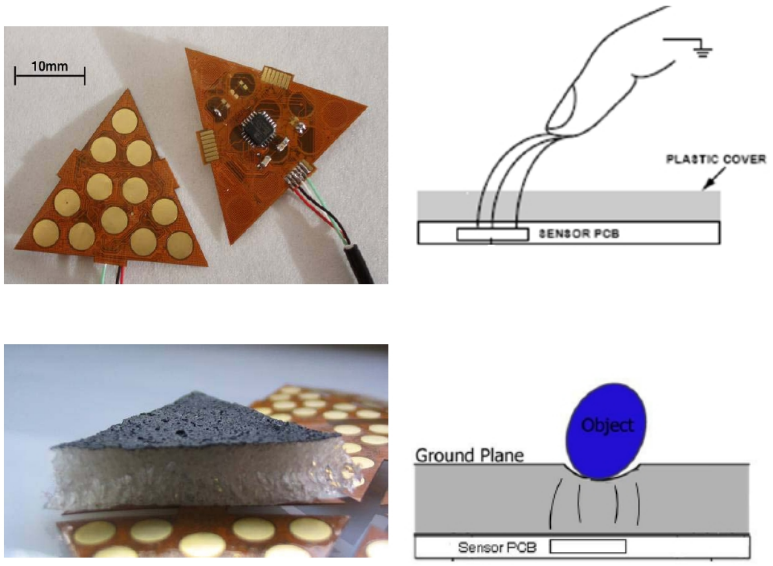

(a) (b)

Figure 1.4. (a) Images and (b) working principle of the triangular structures with the silicone foam fabricated by Cannata *et al* [21].

[23, 24, 25]. Normally the top electrode pattern is deposited on a flexible polymer spinned on a fixed bottom electrode [26, 27, 28, 29], otherwise a cavity between the two electrodes is created, with the use of a sacrificial layer, and air is used as dielectric medium [30, 31]. With these approaches the spatial resolution requirements of 1 mm for fingertips sensor can be overcome easily and capacitor elements of 50 μm square have already been produced with on-chip signal conditioning to observe fine texture as a fingerprint [26].

The drawback of this MEMS technique is the area limitation, since the dimension of the chips is normally limited to few cm^2. Different solution for large area coverage have been proposed using different approaches. One example of fabrication of an artificial skin for covering the whole body of a humanoid robot was made by Cannata *et al.*, combining several sensors interconnected in order to form a networked structure [21]. Each sensor is constituted by a triangular flexible PCB, in order to conform to smooth curved surfaces, with a microcontroller board equipped with a capacitance to digital converter (CDC) on one side and 12 circular capacitive taxels deposited on the other one (see Fig.1.4(a)). A deformable conductive ground plane was added on the sensing side by spraying a thin layer of electrically conductive silicon rubber (connected to ground) on a compliant substrate made

of silicone rubber foam. Under the pressure of an object, the deformation of the ground plane modifies the capacitance value of the circuit, while for human his capacitance is added to the device one as shown in Fig.1.4(b).

Normally large area devices defect in pressure sensitivity. An interesting and effective solution to overcome this problem was proposed by Mannsfeld *et al.*, miming the design of the human skin, combining silicon micromachining and polymer moulding [32]. In order to reproduce the ridges of human skin, different patterns organized in an array structure were fabricated on a Si wafer, later used for molding the surface topology on a PDMS film working as dielectric layer (Fig.1.5). The sensing skin presented an elevate pressure sensitivity, tunable by using different microstructures, with a maximum value of 0.55 kPa^{-1}, reached with the pyramids one.

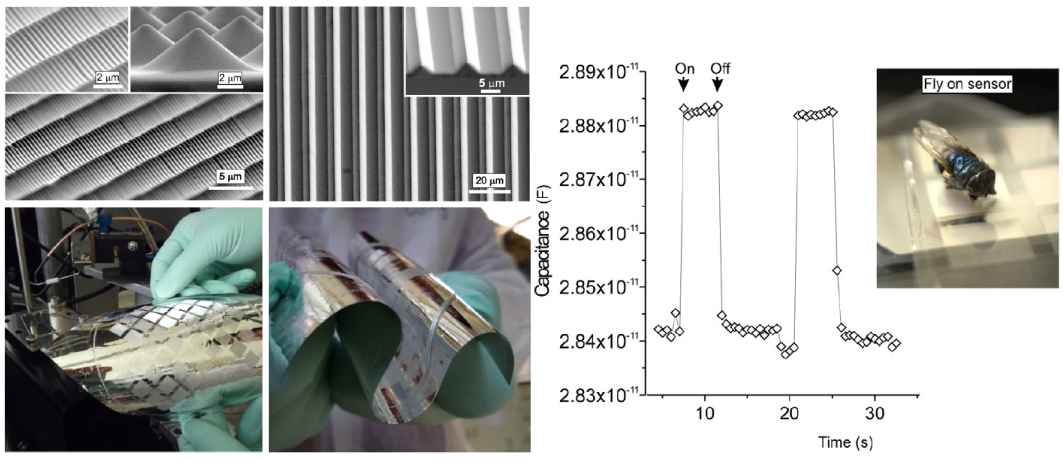

(a) (b)

Figure 1.5. (a) Top: Scanning Electron Microscopy (SEM) images of micro-structured PDMS films with pyramid or line features. Bottom: Pressure sensitive PDMS thin film moulded from a whole microstructured wafer (diameter 100 mm). (b) Variation of the sensor capacitance placing and removing a bluebottle fly 20 mg weight on an area of 64 mm^2. The device was able to sense a pressure of 3 Pa [32].

Summarizing capacitive techniques ensures very high sensitivity, temperature independence, small sizes and high spatial resolution, but also the possibility of a large area coverage. The main drawbacks are stray capacitances, severe hysteresis, electromagnetic sensitivity and cross-talk phenomena.

1.3.2 Optical sensors

Optical transduction mode takes advantage from changes in light intensity to measure deformations. The use of optical fibers to carry the signals considerably reduces the wiring complexity and cross talk. The simplest system are constituted by a LED source, a CCD camera and plastic optical fibers. Variation of light intensity from the source to the detector are generated by a deformation of the fibers [33] or a movement of reflector chips [34]. These systems are immune to electromagnetic interference, flexible, highly sensitive (they can sense few tens of mN), and fast, but they are bulky because of the optical cables.

Devices based on LEDs used both as transmitter and detector guarantee smaller and cheaper solutions that can conform to complex curve surfaces due to the possibility of being fabricated on flexible substrate. The LEDs are placed on the same layer covered by a polymeric film, acting as sensing skin, that deforms under the application of a force. Hence one LED emits light to the upper surface of the skin, while the other one detects the reflected light which intensity depends on the induced deformation of the flexible layer [35, 36].

An interesting and effective solution to obtain a spacial resolution far beyond 1 mm was proposed by Maheshwari e Saraf [37]. Applications like minimum invasive surgery and cancer detection require a level of sophistication much higher than humanoid robotic. For this reason they fabricated a tactile sensor able to detect features with a resolution higher than 20 μm and sensitivity of 10 kPa, by combining metal and semiconducting nanoparticles. The device consists of alternating layer of gold (Au) and cadmium sulfide (CdS) separated by dielectric layers. Applying a voltage across the film, a tunnelling electron current flows through the film inducing the CdS nanoparticles to emit light at a wavelength of 580 nm. By applying a load the dielectric layers become compressed and the particles get closer, thus increasing the tunnelling current and the intensity of the emitted light (linear dependence with stress). Fig.1.6 shows the stress images obtained by pressing an object on the device, with different pressure, and focusing the resulting electroluminescent light directly on the CDD detector.

Optical tactile sensing guarantees low wiring, no cross-talk phenomena, high sensitivity, flexibility and low cost if using LEDs as source and detector. On the contrary most of the devices have a complex architecture, are bulky, require a long signal elaboration and among all suffer of signal distortion related to loss of light by microbending and misalignment.

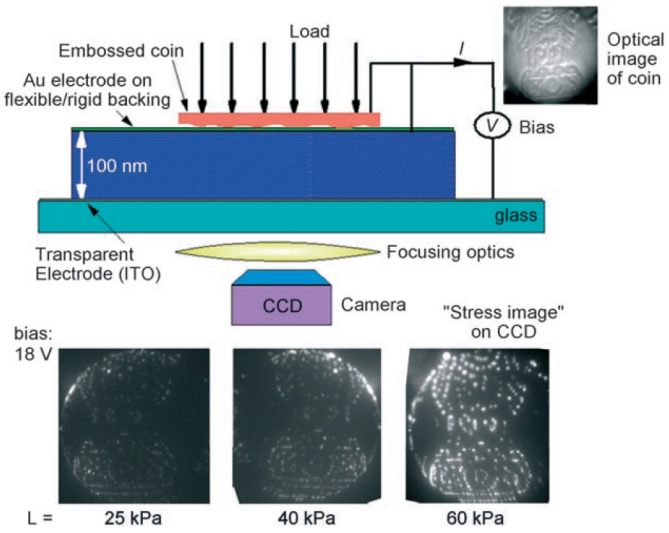

Figure 1.6. Schematic of the optical tactile sensor measuring the load applied on an Indian 5 Rupee and stress images obtained at different pressures applying a bias of 18 V [22]

1.3.3 Piezoelectric sensors

Piezoelectric materials generate an electrical potential gradient when they are mechanically deformed by an applied force [38]. Generally the sensitivity is very high since even nanometric deformations can create potentials in the range of few volts. However, since the voltage output decreases with time, these sensors are only suitable for dynamic tactile sensing [39].

The basic design of a piezoelectric taxel is similar to the capacitive one, with a thin layer of piezoelectric material placed between two conductive electrodes. Under the effect of a force, the electric dipoles of the material move generating charges at the two electrodes, thus a potential across the taxel. The magnitude of the generated charges depends on the ratio between the piezoelectric constant d_{33} of the material and its dielectric constant ε_r [40].

Many different materials have been used in piezoelectric tactile devices, but among all lead zirconate titanate (PZT) and polyvinylidene fluoride (PVDF) were the most implemented ones. PZT has the highest piezoelectric constant among piezoelectric material (commercial PZT with d_{33} above 700 pC/N are commercially available [41, 42]) and its electrical and mechanical properties can be modified by doping. PVDF and its copolymer P(VDF-trifluoroethylene) have much lower piezoelectric constant (d_{33} around 30 pC/N), but at the same time a lower value of dielectric constant (even 100 times lower than PZT)

that guarantees very high sensitivity [43]. Moreover since these polymers are low cost, ease to process, mechanical flexible and chemical inert, they become so widely diffused to exceed the use of ceramic material in piezoelectric tactile sensing [44, 45].

Thanks to the higher workability, the sensitivity of the PVDF tactile sensors was increased by processing the material with micromachining techniques. An example are the devices fabricated with dome and bump shape (PVDF-TrFE) films by Li *et al.* [46]. The completely flexible tactile sensors showed a high sensitivity, due to the polymer microstructuration (see Fig.1.7), which can measure forces as small as 40 mN for bump shape sensors and 25 mN for dome shape sensors. In addition, to reduce crosstalk among different taxels, a selective DC poling method for the PVDF-TrFE film was developed.

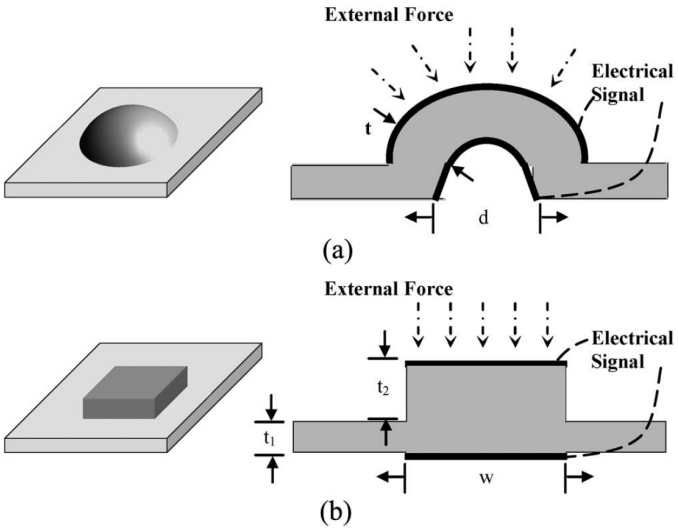

Figure 1.7. Schematic and working principle of the dome and bump shape PVDF-TrFE tactile sensors. (a) Dome shape (t = 30 μm; d = 500 μm, 1 mm, and 1.5 mm). (b) Bump shape (t1 = 10 μm; t2 = 20 μm; w = 500 μm, 1mm, and 1.5 mm) [46].

Dahiya *et al.* proposed different architectures of piezoelectric sensor arrays to measure the force and partially process the signal at the same site, miming the work of human mechanoreceptors. A first design consisted of microelectrode array of 32 elements (1 mm center to center distance), with a sensing film of PVDF-TrFE deposited onto the top of the metal disks (see Fig.1.8(a)) [47]. The taxels showed a linear response to applied forces in the range of 0.02-4 N, with a sensitivity of 0.2 V/N and 0.4 V/N depending on the sensing film thickness. Drawback of this design was the cross-talk between the sensors. The

second devices was composed by an array of POSFET (Piezoelectric Oxide Semiconductor Field Effect Transistor) [48]. By spinning the piezoelectric polymer film directly onto field emitting transistors (FETs), they succeeded in unifying the sensing element and the processing circuitry in an unique entity, decreasing processing time and reducing cross-talk (see Fig.1.8(b)). Each POSFET had an area of 1 mm^2 and a linear response in the range of 0.2-5 N with a sensitivity of 0.5 V/N.

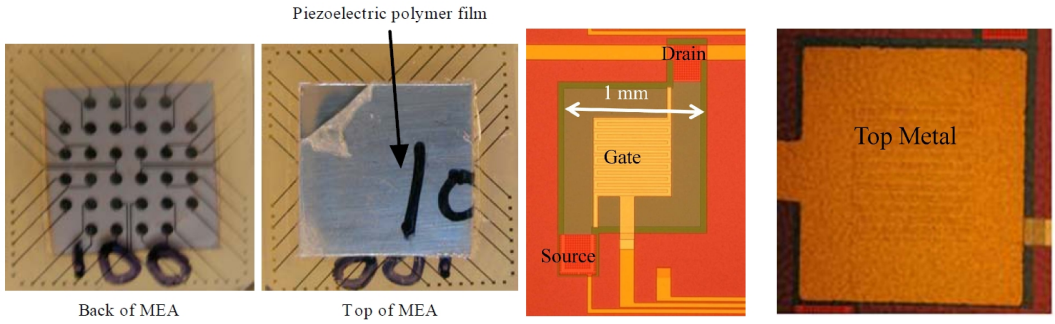

Figure 1.8. (a) Back and top sides of the microelectrode array with 100 μm piezoelectric film (with a protecting tape on top of polymer) [47] and (b) images of a POSFET device before and after the deposition of the PVDF-TrFE film [48].

Piezoelectric tactile sensors can guarantee a high sensitivity, fast response, low dimensions and high bandwidth and, in particular referred to PVDF based devices, flexibility, robustness and chemical inertness. However, they are only suitable for dynamic application, suffer of drift of the output voltage, fragility of the electrical junctions and temperature sensitivity.

1.3.4 Magnetic sensors

Magnetic tactile sensors correlate a change in flux density with the the deformation induced by an applied force. The variation of the magnetic flux can be measure by Hall-effect [49] or magnetoresistive device [50].

An example of the first subfamily is the device proposed by Jamone *et al.* and mounted on the humanoid robot called James [49]. The sensor structure, shown in Fig.1.9(a), consists of a small cylindric magnet dip in a silicone cover, separate by the Hall-effect sensor by an air gap to increase the rubber deformation and magnet displacement (i.e. increase sensitivity). In fact any external pressure on the silicone surface causes a movement of the magnet

and therefore a change in the magnetic field sensed by the Hall-effect sensor. Two kinds of sensors were fabricated, depending on the mounting location (Fig.1.9(b)). Phalangeal-sensors, for some of the phalanxes, had only one sensing element which resulted in a limited range of forces and was used as an on/off response. On the contrary fingertip-sensors, for the distal ends of each finger, had two sensing elements capable of sensing a larger range of applied pressure. Finally twelve tactile sensors were mounted on the robot hand: 5 fingertip-sensors, one for each finger, and 7 phalangeal-sensors, two on the thumb, ring finger and middle finger, and one on the index finger. This architecture had a very high sensitivity, with a minimum force intensity detectable of less than 10 grams for fingertip-sensors and about 2 grams for phalangeal-sensors, but the response was not-linear.

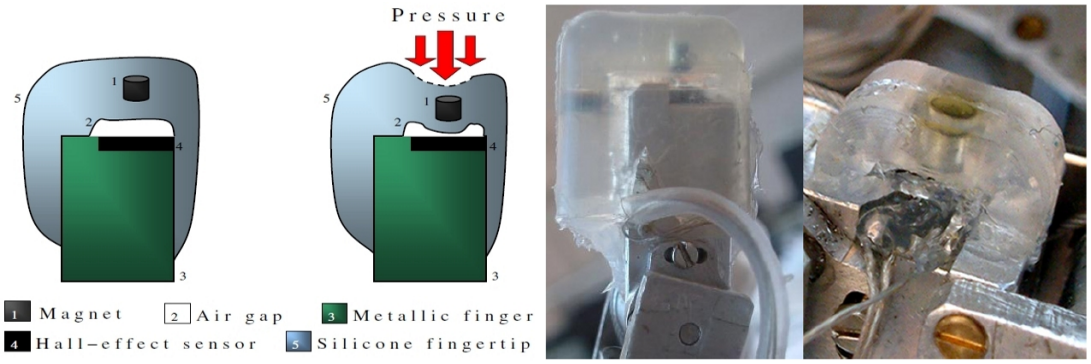

(a) (b)

Figure 1.9. (a) Working principle of the magnetic tactile devices using on Hall-effect sensors. (b) Images of the fingertip-sensor (left) with two sensing elements and phalangeal-sensor (right) with only one element [49].

Devices based on magnetic principle have high sensitivity, large dynamic range, no measurable mechanical hysteresis, and physical robustness. However, they have several drawbacks because the usage is limited to nonmagnetic mediums, they are bulky and with elaborate architectures and require complex computations.

1.3.5 Ultrasonic sensors

Acoustic ultrasonic principle has been widely used in research and commercially in all the areas of sensing (such as chemical, optical, thermal, pressure, acceleration, torque and biological) [51, 52]. In fact acoustic waves, generated in a piezoelectric medium, modify their frequency, phase, amplitude or time-delay under the effect of an external stimulus.

Ultrasonic tactile sensing devices were fabricated to detect the variation in piezoelectric resonance frequency with the applied pressure. Most of the sensors use ceramic materials like lead zirconate titanate (PZT), which are fragile and difficult to process in MEMS technology [53]. in contrast using flexible piezoelectric polymers, such as polyvinylidene fluoride (PVDF), both as emitter and receiver to localize and detect contact force, slip, friction and surface roughness surface can greatly simplify such difficulties [54, 55]. Moreover by exploiting the different acoustic impedance of the objects, when they come in contact with the sensor, is possible to detect beyond the applied force, even mechanical properties like hardness and softness [56].

Summarizing, ultrasonic sensors have a good pressure sensitivity, fast response and are made with a well consolidated technology. The drawbacks are fragility, hysteresis and compensation of secondary effect modifying the generated waves, since they are very sensible to the external stimuli such temperature, humidity, etc.

1.3.6 Resistive sensors

Last in order of appearance, but probably the most important,the resistive sensors is certainly the most studied family of device, with the highest number of reported applications. Under the effect of an applied force/pressure the sensor varies its resistance. This could be determined by a geometric change, as in strain gauges, by a resistivity variation, as in piezoresistors, or by both the effect, that is the most common case.

1.3.6.1 Strain gauges

Strain gauges are typically metal long winding snake-like structures on an insulator plane that when deformed increases its length, thus decreasing the cross section and modifying the whole resistance. On the contrary, the strain is not significantly affecting the electron mobility in metals, thus the resistivity variation is negligible [57].

Several examples of micromachined arrays of strain gauges were fabricated with an elevate sensitivity, but most of all are rigid and fragile [58, 59]. Upon embedding the MEMS structures into polymeric layers, it is possible to increase the flexibility and the robustness, but the sensitivity results lowered. An interesting example was fabricated by Noma group orthogonally placing strain gauges on silicon-based microcantilevers, embedded in a layer of flexible polymer, as shown in Fig.1.10 [60]. In this way, the sensitivity of the strain gauges

increased since they detected the deformation both of the cantilevers and of the elastomer due to applied stress. Moreover by evaluating the output of each cantilever it was possible to discriminate between normal and shear stresses, with a maximum sensitivity of 0.6%/N using polyurethane as polymeric material.

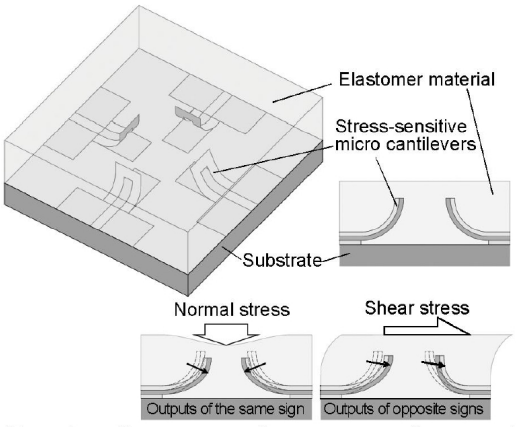

Figure 1.10. Schematic and working principle of the three axial tactile sensor with strain gauges [60].

Strain gauges have high sensitivity, small size and ease integration in MEMS devices and on PCB, but have several disadvantages like fragility, costly material, temperature sensitivity and rigidity. These drawbacks can be overcome by embedding the strain gauges in flexible polymers, even obtaining devices with the possibility of 3D sensing, but they will loose in sensitivity and become bulky.

1.3.6.2 MEMS piezoresistors

In piezoresistors stress induces a variation of the resistivity of the material itself. To minimize the dimension and produce a large number of sensing elements, MEMS technology exploits the high piezoresistive responses of silicon and other semiconductor (as germanium). In fact in semiconductor the stress modifies the width of the band gap and consequently the mobility of the charge carriers (electrons and holes). Then a significant variation of the resistivity is induced because of the dependence on mobility and the density of the charge carriers [57]. Like the strain gauges, these piezoresistors are fragile and rigid, while embedded in elastomer they increase their flexibility at the expense of sensitivity.

Valdestri *et al.* fabricated a three-axial silicon based MEMS force sensor [61]. The sensing part, shown in Fig.1.11(a), was a silicon high aspect-ratio structure with an integrated silicon plane cylinder used for the transmission of the force to a flexible tethered structure. The magnitude and the direction of the force was measured by four independent bar shaped p-type silicon piezoresistors, placed at the tether roots. The experimental sensitivity in the shear directions was 0.054/N and in the normal direction 0.026/N.

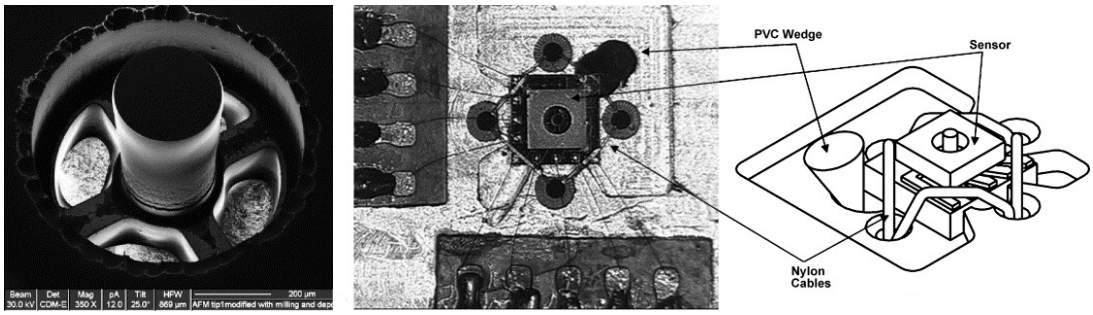

(a) (b)

Figure 1.11. (a) Focus ion beam (FIB) image of the MEMS sensing part and (b) top view and schematic of a sensor taxel [61].

Semiconducting piezoresistors are similar to strain gauges for what concerns advantages and disadvantages, but the positive aspect is that they can have much smaller dimension, since they do not need snake-like shapes, and achieve a larger number of sensing elements per area.

1.3.6.3 Piezoresistive polymers and fabrics

Devices of this family are flexible, mechanically robust, and chemically resistant (depending on the polymer used). The spatial resolution is generally low, but since they can be fabricated with low cost and large area techniques such as screen printing, moulding or roll-to-roll, they are suitable for large area tactile sensing [62]. In piezoresistive polymers, a deformation induces a re-arrangement of the polymeric chains modifying the conduction properties [63, 64], while in fabrics the stress over the conductive robot knit causes a local change in the contact resistance of the yarns, modifying the resistance distribution in the sheet.

One of the most remarkable examples of this transduction method applied to a tactile

sensing area was proposed by Alirezaei *et al* [65]. They fabricated a large area tactile sensors, with a layer of conductive fabric, based on EIT (Electrical Impedance Tomography) which was capable of detecting mechanical stimuli such as touch, pressure and stretch. The resistance of the material, alterable by deformations, was measured by applying a current between the electrodes, flowing through the whole conductive sheet and generating an electrical potential distribution. The sensor was extremely stretchable and flexible, suitable for covering delicate and complex 3D-surfaces of the robot body such as the face, arms and shoulder (see Fig.1.12) The device had a spatial resolution of 9 mm and force threshold of 20 N. These characteristics are low for utilization on fingertips or palm, but acceptable for large area tactile sensing.

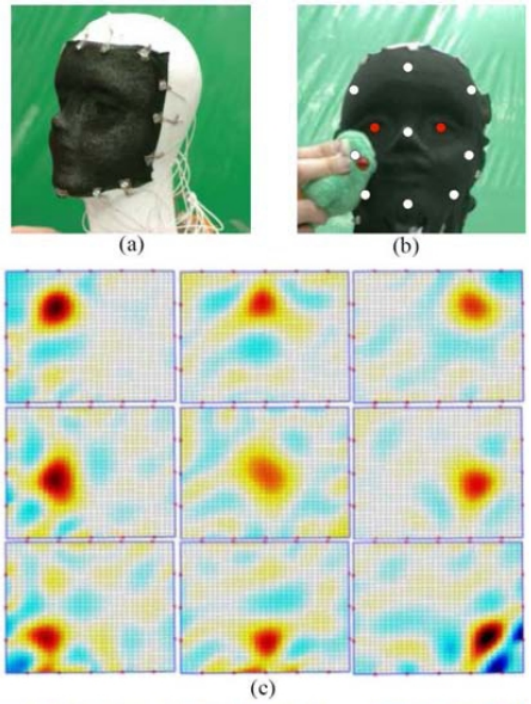

Figure 1.12. (a) Fabric tactile sensor applied on a dummy face, (b) point of application of the pressure (red points represent the eyes) and (c) measures of the above-mentioned points [65].

As already said above, polymer and fabric sensors have optimum mechanical properties such as flexibility and robustness, they are low cost and posses simple structures, but also have a low sensitivity and spatial resolution.

1.3.6.4 Piezoresistive composite materials

Composite polymeric materials with piezoresistive properties are one of the best candidates to make a sensing "skin" able to reproduce the tactile sense and to fit the shape of the robot structure. Beyond the high conformability, these sensing materials have usually a wide range of sensitivity, a low power consumption and an elevate mechanical resistance, protecting the system from overpressure, shock and vibrations [66]. In order to tune the properties of the composite and the working range of the sensor, several different conductive particles have been used as filler for hybrid piezoresistive materials, e.g. carbon black, graphite flakes, carbon nanotubes, semiconducting metal-oxides and various metal powders [67, 68, 69, 70]. By varying the type and amount of fillers, the composite can assume the electrical properties of an insulator up to those of a good conductor. Even the choice of the insulating polymeric matrix (e.g., silicones, polyurethane, acrylics, etc.) strongly influence the mechanical and electrical behaviour of the composite [66, 67, 71]. Anyway, the basic working principle is the same in all the composites: a mechanical deformation of the polymeric matrix alters the local spatial distribution of the filler particles changing the electrical resistance of the whole material. Therefore this variation can be directly correlated to the applied force to the composite.

Most of the composites consist of conductive filler particles in an insulating polymer matrix and becomes conductive when the volume fraction of the particles is above a certain value, the percolation threshold. Above this limit at least one channel of conductive particles is created across the sample and forms a conducting (percolating) pathway, as better described in chapter 2. This value is affected by the shape of the fillers and can be even below 1% for fiber-like particles such as carbon nanotubes or whiskers [72, 73]. Under the effect of a compressive force, the particles come closer because of the deformation of the polymeric matrix, increasing the number of percolating channels, thus lowering the resistance of the material.

Hundreds examples of tactile devices exploiting the percolation phenomenon in composites have been presented. A novel architecture was proposed by Cheng *et al.* to fabricate an anthropomorphic robot skin with a large area 16 x 16 highly stretchable tactile sensing arrays [74]. PDMS was employed both for the fabrication of the the skin structure and as matrix of the piezoresistive conductive composite with carbon black, copper and silver powder as fillers (see Fig.1.13). The sensing material was placed at the crossing of orthogonally spiral electrodes that can withstand high deformation and twisting. Another interesting

design is the coupling of the piezoresistive composites with flexible organic field effect transistor (OFET) that integrates a sensor element with the acquisition electronics [75]. For a fixed gate voltage, when the resistance of the composite decreases the source-drain voltage proportionally increases. This configuration guarantees a high sensitivity and a much lower power consumption compared to the classical device which simply measuring the electrical resistance.

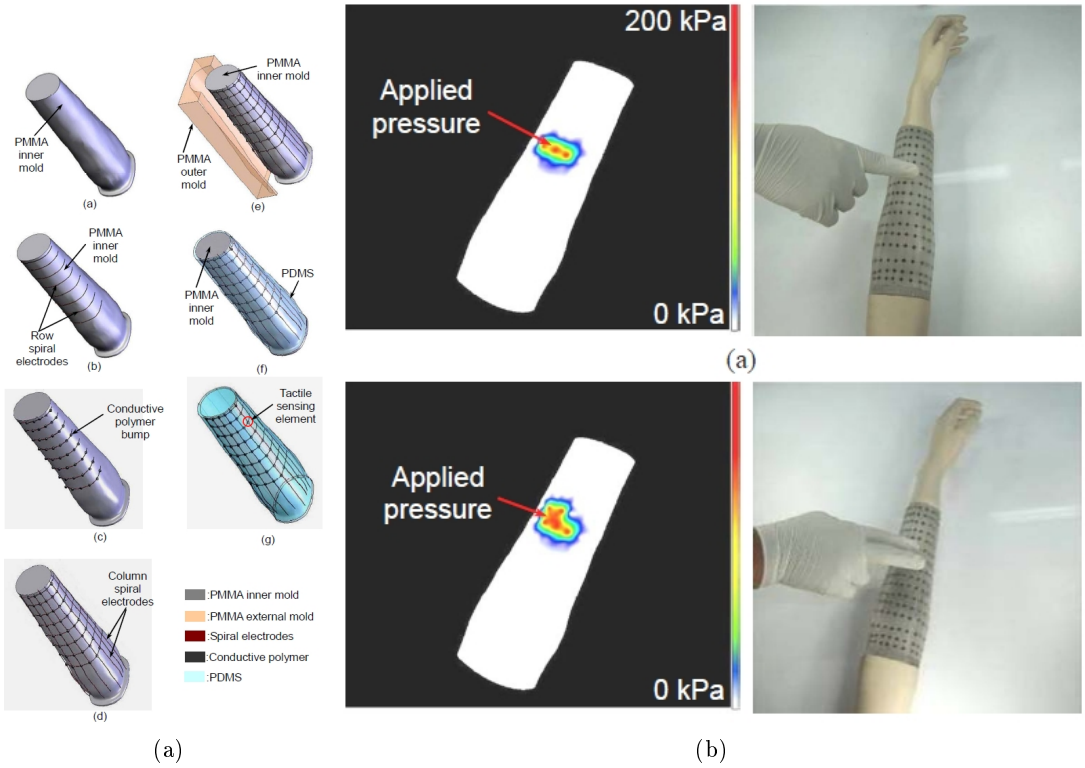

Figure 1.13. (a) Process flow of the fabrication of the large area tactile sensor with arm shape and (b) measurements of two different pressure distributions [74].

One of the major disadvantages of the percolation composite is the low dynamic range. This problem is successfully overcome in piezoresistive composite material based on tunnelling conduction mechanism, even with a further increase of the sensitivity. In these composites a small variation of the external load induces a huge change of the electrical conductivity [76, 77, 78]. The main difference with respect to the previously described composites is that, even above the percolation threshold, each conductive particles is separated

from the others by a thin layer of insulating polymer representing the tunneling barrier, without creating a percolation path [79]. This effect is due to the particular shape of the fillers, presenting sharp and nanostructured tips on the surface that allows the polymer to completely cover the particles. When the material is compressed, stretched or twisted, the mechanical deformation induces a reduction of the polymer thickness, thus decreasing the tunneling barrier. As a consequence, the probability of tunneling phenomena increases, resulting in a large reduction of the bulk electrical resistance. The first material exploiting these properties was presented by Bloor *et al.* [76] mixing nickel particles in an elastomeric matrix, and subsequently a tactile device fabricated with QTC was implemented on NASA Robonaut (see Fig.1.14) [80].

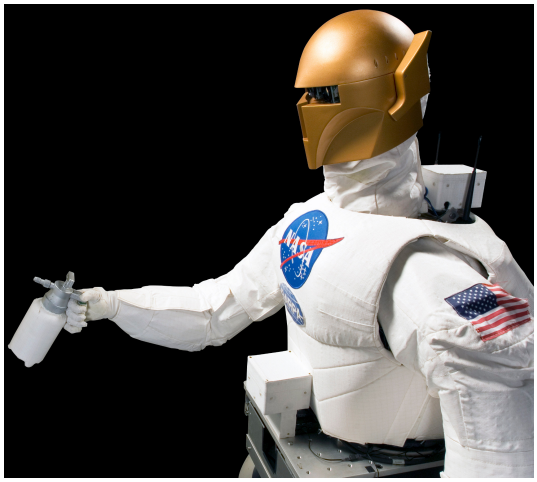

Figure 1.14. Image of Robonaut [80].

Summarizing piezoresistive composite material have very low cost, high sensitivity, mechanical flexibility and simple structure and electronics. The negative aspects are the hysteresis of the material, the high power consumption (depending on the resistance value and successfully reduced in OFET system) and low sensing range (increased in tunnelling based composites).

Bibliography

[1] H. Yousef, M. Boukallel, and K. Althoefer. Tactile sensing for dexterous in-hand manipulation in robotics - A review. *Sensors and Actuators, A: Physical*, 167(2):171–187,

2011.

[2] R.S. Dahiya, G. Metta, M. Valle, and G. Sandini. Tactile Sensing-From Humans to Humanoids. *Robotics, IEEE Transactions on*, 26(1):1–20, 2010.

[3] M.R. Cutkosky, R.D. Howe, and W.R. Provancher. Force and tactile sensors. In *Springer Handbook of Robotics*, pages 455–476. Springer Berlin Heidelberg, 2008.

[4] T.D. Crouch. *Wings: A History of Aviation from Kites to the Space Age*. New York: Norton, 2003.

[5] S.D. Strauss. *The Big Idea: How Business Innovators Get Great Ideas to Market*. Dearborn Trade Pub., 2002.

[6] J.M. Loomis and S.J. Lederman. Cognitive processes performances. In *Handbook of Perception and Human Performances Series*, volume 2. New York: Wiley, 1986.

[7] M.S.A. Graziano and M.M. Botvinick. How the brain represents the body: Insights from neurophysiology and psychology. In *Attention and performance: Vol. XIX. Common mechanisms in perception and action*, pages 136–157. London, U.K.: Oxford Univ. Press, 2002.

[8] R.L. Klatzky and S.J. Lederman. Touch. In *Handbook of Psychology*, volume 4, pages 147–176. New York: Wiley, 2002.

[9] I. Birznieks, P. Jenmalm, A.W. Goodwin, and R.S. Johansson. Encoding of direction of fingertip forces by human tactile afferents. *Journal of Neuroscience*, 21(20):8222–8237, 2001.

[10] H. Athenstaedt, H. Claussen, and D. Schaper. Epidermis of human skin: Pyroelectric and piezoelectric sensor layer. *Science*, 216(4549):1018–1020, 1982.

[11] R.S. Johansson and G. Westling. Roles of glabrous skin receptors and sensorimotor memory in automatic control of precision grip when lifting rougher or more slippery objects. *Experimental Brain Research*, 56(3):550–564, 1984.

[12] B.B. Edin, L. Ascari, L. Beccai, S. Roccella, J.-J. Cabibihan, and M.C. Carrozza. Bio-inspired sensorization of a biomechatronic robot hand for the grasp-and-lift task. *Brain Research Bulletin*, 75(6):785–795, 2008.

[13] E.R. Kandel, J.H. Schwartz, and T.M. Jessell. *Principles of Neural Science*. New York: McGraw-Hill Medical, 1991.

[14] J.M. Wolfe, K.R. Kluender, D.M. Levi, L.M. Bartoshuk, R.S. Herz, R.L. Klatzky, and S.J. Lederman. *Sensation & Perception*. Sunderland, MA: Sinauer, 2006.

[15] L.A. Jones and S.J. Lederman. Tactile Sensing. In *Human Hand Function*, pages 44–74. Cambridge, MA: Oxford Univ. Press, 2006.

[16] J. Dargahi and S. Najarian. Human tactile perception as a standard for artificial tactile sensing–a review. *The international journal of medical robotics + computer assisted surgery : MRCAS*, 1(1):23–35, 2004.

[17] R.S. Dahiya and M. Valle. Tactile sensing: Definitions and classification. In *Robotic Tactile Sensing*, pages 13–17. Springer Netherlands, 2013.

[18] J.A. Gálvez, P.G. De Santos, and F. Pfeiffer. Intrinsic tactile sensing for the optimization of force distribution in a pipe crawling robot. *IEEE/ASME Transactions on Mechatronics*, 6:26–35, 2001.

[19] P. Mittendorfer and G. Cheng. Humanoid multimodal tactile-sensing modules. *IEEE Transactions on Robotics*, 27:401–410, 2011.

[20] G. De Maria, C. Natale, and S. Pirozzi. Force/tactile sensor for robotic applications. *Sensors and Actuators A: Physical*, 175:60–72, 2012.

[21] G. Cannata, M. Maggiali, G. Metta, and G. Sandini. An embedded artificial skin for humanoid robots. In *IEEE International Conference on Multisensor Fusion and Integration for Intelligent Systems*, pages 434–438, 2008.

[22] V. Maheshwari and R. Saraf. Tactile devices to sense touch on a par with a human finger. *Angewandte Chemie - International Edition*, 47:7808–7826, 2008.

[23] W.P. Eaton and J.H. Smith. Micromachined pressure sensors: Review and recent developments. *Smart Materials and Structures*, 6:530–539, 1997.

[24] J.W. Judy. Microelectromechanical systems (MEMS): Fabrication, design and applications. *Smart Materials and Structures*, 10:1115–1134, 2001.

[25] B.L. Gray and R.S. Fearing. Surface micromachined microtactile sensor array. In *Proceedings - IEEE International Conference on Robotics and Automation*, volume 1, pages 1–6, 1996.

[26] N. Sato, S. Shigematsu, H. Morimura, M. Yano, K. Kudou, T. Kamei, and K. Machida. Novel surface structure and its fabrication process for MEMS fingerprint sensor. *IEEE Transactions on Electron Devices*, 52:1026–1032, 2005.

[27] J.N. Palasagaram and R. Ramadoss. MEMS-capacitive pressure sensor fabricated using printed-circuit-processing techniques. *IEEE Sensors Journal*, 6:1374–1375, 2006.

[28] K. Arshak, E. Jafer, and A. Fox. Design of a new thick film capacitive pressure and circuitry interface. *Composites Science and Technology*, 65:757–764, 2005.

[29] R.J. De Souza and K.D. Wise. Very high density bulk micromachined capacitive tactile imager. In *International Conference on Solid-State Sensors and Actuators, Proceedings*, volume 2, pages 1473–1476, 1997.

[30] A.V. Chavan and K.D. Wise. Batch-processed vacuum-sealed capacitive pressure sensors. *Journal of Microelectromechanical Systems*, 10(4):580–588, 2001.

[31] Y. Zhang, R. Howver, B. Gogoi, and N. Yazdi. A high-sensitive ultra-thin mems capacitive pressure sensor. In *2011 16th International Solid-State Sensors, Actuators and Microsystems Conference, TRANSDUCERS'11*, pages 112–115, 2011.

[32] S.C.B. Mannsfeld, B.C.-K. Tee, R.M. Stoltenberg, C.V.H.-H. Chen, S. Barman, B.V.O. Muir, A.N. Sokolov, C. Reese, and Z. Bao. Highly sensitive flexible pressure sensors with microstructured rubber dielectric layers. *Nature Materials*, 9(10):859–864, 2010.

[33] J.-S. Heo, J.-Y. Kim, and J.-J. Lee. Tactile sensors using the distributed optical fiber sensors. In *Proceedings of the 3rd International Conference on Sensing Technology, ICST 2008*, pages 486–490, 2008.

[34] Y. Yamada, T. Morizono, Y. Umetani, and H. Takahashi. Highly soft viscoelastic robot skin with a contact object-location-sensing capability. *IEEE Transactions on Industrial Electronics*, 52(4):960–968, 2005.

[35] J. Rossiter and T. Mukai. An led-based tactile sensor for multi-sensing over large areas. In *Proceedings of IEEE Sensors*, pages 835–838, 2006.

[36] Y. Ohmura, Y. Kuniyoshi, and A. Nagakubo. Conformable and scalable tactile sensor skin for a curved surfaces. In *Proceedings - IEEE International Conference on Robotics and Automation*, volume 2006, pages 1348–1353, 2006.

[37] V. Maheshwari and R.F. Saraf. High-resolution thin film device to sense texture by touch. *Science*, 312(5779):1501–1504, 2006.

[38] W.G. Cady. *Piezoelectricity*. McGraw-Hill, New York, 1946.

[39] P. Puangmali, K. Althoefer, L.D. Seneviratne, D. Murphy, and P. Dasgupta. State-of-the-art in force and tactile sensing for minimally invasive surgery. *IEEE Sensors Journal*, 8(4):371–380, 2008.

[40] J. Sirohi and I. Chopra. Fundamental understanding of piezoelectric strain sensors. *Journal of Intelligent Material Systems and Structures*, 11(4):246–257, 2000.

[41] www.piezotechnologies.com/Ceramics/quick-selection chart.aspx.

[42] D.L. Polla and L.F. Francis. Processing and characterization of piezoelectric materials and integration into microelectromechanical systems. *Annual Review of Materials Science*, 28(1):563–597, 1998.

[43] A.J. Lovinger. Ferroelectric polymers. *Science*, 220(4602):1115–1121, 1983.

[44] P. Ueberschlag. PVDF piezoelectric polymer. *Sensor Review*, 21(2):118–125, 2001.

[45] S.B. Lang and S. Muensit. Review of some lesser-known applications of piezoelectric and pyroelectric polymers. *Applied Physics A: Materials Science and Processing*, 85:125–134, 2006.

[46] C. Li, P.-M. Wu, S. Lee, A. Gorton, M.J. Schulz, and C.H. Ahn. Flexible dome and bump shape piezoelectric tactile sensors using PVDF-TrFE copolymer. *Journal of Microelectromechanical Systems*, 17(2):334–341, 2008.

[47] R.S. Dahiya, M. Valle, G. Metta, L. Lorenzelli, and C. Collini. Tactile sensing arrays for humanoid robots. In *Proceedings of the 2007 Ph.D Research in Microelectronics and Electronics conference, PRIME 2007*, pages 201–204, 2007.

[48] R.S. Dahiya, M. Valle, G. Metta, L. Lorenzelli, and A. Adami. Design and fabrication of posfet devices for tactile sensing. In *TRANSDUCERS 2009 - 15th International Conference on Solid-State Sensors, Actuators and Microsystems*, pages 1881–1884, 2009.

[49] L. Jamone, G. Metta, F. Nori, and G. Sandini. James: A humanoid robot acting over an unstructured world. In *Proceedings of the 2006 6th IEEE-RAS International Conference on Humanoid Robots, HUMANOIDS*, pages 143–150, 2006.

[50] T.J. Nelson, R.B. van Dover, S. Jin, S. Hackwood, and G. Beni. Shear-sensitive magnetoresistive robotic tactile sensor. *IEEE Transactions on Magnetics*, MAG-22(5), 1986.

[51] A. Pohl. A review of wireless saw sensors. *IEEE Transactions on Ultrasonics, Ferroelectrics, and Frequency Control*, 47(2):317–332, 2000. cited By (since 1996) 144.

[52] B. Drafts. Acoustic wave technology sensors. *IEEE Transactions on Microwave Theory and Techniques*, 49(4 II):795–802, 2001.

[53] G.M. Krishna and K. Rajanna. Tactile sensor based on piezoelectric resonance. *IEEE Sensors Journal*, 4(5):691–697, 2004.

[54] Shigeru Ando and Hiroyuki Shinoda. Ultrasonic emission tactile sensing. *IEEE Control Systems Magazine*, 15(1):61–69, 1995.

[55] K. Nakamura and H. Shinoda. A tactile sensor instantaneously evaluating friction coefficients. *Proc. of the 11th Int. Conf. on Solid-state Sensors and Actuators*, 2:1430–1433, 2001.

[56] S. Omata, Y. Murayama, and C.E. Constantinou. Real time robotic tactile sensor system for the determination of the physical properties of biomaterials. *Sensors and Actuators, A: Physical*, 112(2-3):278–285, 2004.

[57] C.S. Smith. Piezoresistance effect in germanium and silicon. *Physical Review*, 94(1):42–49, 1954.

[58] K. Kim, K.R. Lee, W.H. Kim, K.B. Park, T.H. Kim, J.S. Kim, and J.J. Pak. Polymer-based flexible tactile sensor up to 32 x 32 arrays integrated with interconnection terminals. *Sensors and Actuators, A: Physical*, 156(2):284–291, 2009.

[59] J. Engel, J. Chen, and C. Liu. Development of polyimide flexible tactile sensor skin. *Journal of Micromechanics and Microengineering*, 13(3):359–366, 2003.

[60] Y.M. Huang, M. Sohgawa, K. Yamashita, T. Kanashima, M. Okuyama, M. Noda, and H. Noma. Fabrication and normal/shear stress responses of tactile sensors of polymer/Si cantilevers embedded in PDMS and urethane gel elastomers. *IEEJ Transactions on Sensors and Micromachines*, 128(5):193–197, 2008.

[61] P. Valdastri, S. Roccella, L. Beccai, E. Cattin, A. Menciassi, M.C. Carrozza, and P. Dario. Characterization of a novel hybrid silicon three-axial force sensor. *Sensors and Actuators, A: Physical*, 123-124:249–257, 2005.

[62] C. Liu. Recent developments in polymer MEMS. *Advanced Materials*, 19(22):3783–3790, 2007.

[63] Z. Del Prete, L. Monteleone, and R. Steindler. A novel pressure array sensor based on contact resistance variation: Metrological properties. *Review of Scientific Instruments*, 72:1548–1553, 2001.

[64] J. Wang, H. Sato, C. Xu, and M. Taya. Bioinspired design of tactile sensors based on flemion. *Journal of Applied Physics*, 105(8), 2009.

[65] H. Alirezaei, A. Nagakubo, and Y. Kuniyoshi. A highly stretchable tactile distribution sensor for smooth surfaced humanoids. In *Proceedings of the 2007 7th IEEE-RAS International Conference on Humanoid Robots, HUMANOIDS 2007*, pages 167–173, 2008.

[66] S.Y. Fu, X.Q. Feng, B. Lauke, and Y.W. Mai. Effects of particle size, particle/matrix interface adhesion and particle loading on mechanical properties of particulate-polymer composites. *Composites Part B: Engineering*, 39(6):933–961, 2008.

[67] R. Strumpler and J. Glatz-Reichenbach. Conducting polymer composites. *Journal of Electroceramics*, 3(4):329–346, 1999.

[68] M. Knite, V. Teteris, A. Kiploka, and J. Kaupuzs. Polyisoprene-carbon black nanocomposites as tensile strain and pressure sensor materials. *Sensors and Actuators, A: Physical*, 110(1-3):142–149, 2004. cited By (since 1996) 87.

[69] N. Hu, Y. Karube, C. Yan, Z. Masuda, and H. Fukunaga. Tunneling effect in a polymer/carbon nanotube nanocomposite strain sensor. *Acta Materialia*, 56(13):2929–2936, 2008.

[70] Dae-Yong Jeong, Jungho Ryu, Yun-Soo Lim, Shuxiang Dong, and Dong-Soo Park. Piezoresistive TiB2/silicone rubber composites for circuit breakers. *Sensors and Actuators A: Physical*, 149(2):246–250, 2009.

[71] G. Harsányi. Polymer films in sensor applications: A review of present uses and future possibilities. *Sensor Review*, 20(2):98–105, 2000.

[72] J.K.W. Sandler, J.E. Kirk, I.A. Kinloch, M.S.P. Shaffer, and A.H. Windle. Ultra-low electrical percolation threshold in carbon-nanotube-epoxy composites. *Polymer*, 44(19):5893–5899, 2003.

[73] C.A. Martin, J.K.W. Sandler, M.S.P. Shaffer, M.-K. Schwarz, W. Bauhofer, K. Schulte, and A.H. Windle. Formation of percolating networks in multi-wall carbon-nanotube-epoxy composites. *Composites Science and Technology*, 64(15 SPEC. ISS.):2309–2316, 2004.

[74] M.-Y. Cheng, C.-M. Tsao, and Y.-J. Yang. An anthropomorphic robotic skin using highly twistable tactile sensing array. In *Proceedings of the 2010 5th IEEE Conference on Industrial Electronics and Applications, ICIEA 2010*, pages 650–655, 2010.

[75] T. Someya, T. Sekitani, S. Iba, Y. Kato, H. Kawaguchi, and T. Sakurai. A large-area, flexible pressure sensor matrix with organic field-effect transistors for artificial skin applications. *Proceedings of the National Academy of Sciences of the United States of America*, 101(27):9966–9970, 2004.

[76] D. Bloor, K. Donnelly, P. J Hands, P. Laughlin, and D. Lussey. A metal-polymer composite with unusual properties. *J. Phys. D: Appl. Phys.*, 38:2851–2860, 2005.

[77] S. Stassi, V. Cauda, G. Canavese, D. Manfredi, and C.F. Pirri. Synthesis and characterization of gold nanostars as filler of tunneling conductive polymer composites. *European Journal of Inorganic Chemistry*, 16:2669–2673, 2012.

[78] M.K. Abyaneh and S.K. Kulkarni. Giant piezoresistive response in zinc-polydimethylsiloxane composites under uniaxial pressure. *J. Phys. D: Appl. Phys.*, 41:135405, 2008.

[79] G.R. Ruschau, S. Yoshikawa, and R.E. Newnham. Resistivities of conductive composites. *Journal of Applied Physics*, 72(3):953–959, 1992.

[80] T.B. Martin, R.O. Ambrose, M.A. Diftler, R. Platt Jr., and M.J. Butzer. Tactile gloves for autonomous grasping with the nasa/darpa robonaut. In *Proceedings - IEEE International Conference on Robotics and Automation*, volume 2004, pages 1713–1718, 2004.

Chapter 2

Theory of piezoresistive effect in composite materials

The piezoresistivity is the properties of a material to change its electrical resistivity, and therefore the resistance, under the application of a mechanical stress. This effect was discovered by William Thomson, better known as Lord Kelvin, in 1856, measuring through a Wheatstone bridge the resistivity of two telegraphic wires (respectively in copper and iron) subjected to the same loads. He firstly demonstrated that the resistance variation was not due to a geometrical variation, but to a change in the material resistivity.

The electrical resistance R is defined as:

$$R = \rho \frac{l}{S} \tag{2.1}$$

where ρ is the material resistivity and l and S the length and the surface of the sample respectively.

Deriving both the member and moving to finite differences, equation (2.1) becomes:

$$\Delta R = \Delta\rho \frac{l}{S} + \Delta l \frac{\rho}{S} - \Delta S \frac{\rho l}{S^2} \tag{2.2}$$

then dividing by R:

$$\frac{\Delta R}{R} = \frac{\Delta\rho}{R} \frac{l}{S} + \frac{\Delta l}{R} \frac{\rho}{S} - \frac{\Delta S}{R} \frac{\rho l}{S^2} \tag{2.3}$$

and substituting R with " $\rho \frac{l}{S}$ ":

$$\frac{\Delta R}{R} = \frac{\Delta \rho}{\rho} + \frac{\Delta l}{l} - \frac{\Delta S}{S} \tag{2.4}$$

The latter equation can be simplified substituting:

$$\varepsilon = \frac{\Delta l}{l} \tag{2.5}$$

that represents the mechanical strain in the direction parallel to the applied force and:

$$\frac{\Delta S}{S} = -2\nu \frac{\Delta l}{l} = -2\nu\varepsilon \tag{2.6}$$

that represents the variation of the transversal section (with respect to the applied force) for an isotropic and homogeneous material, where ν is the Poisson's ratio. Eqution 2.4 can be finally rewritten as:

$$\frac{\Delta R}{R} = \frac{\Delta \rho}{\rho} + (1 + 2\nu)\,\varepsilon \tag{2.7}$$

where $\frac{\Delta \rho}{\rho}$ is the intrinsic piezoresistivity of the material and $(1 + 2\nu)\,\varepsilon$ the geometrical factor.

Fundamental parameters to quantify the piezoresistive effect are the gauge factor and the piezosensitivity. A precise evaluation of these figures of merit is necessary to compare piezoresistive materials and determine their utilization as functional element in sensor application. The gauge factor GF is the the ratio of relative change in electrical resistance to the applied mechanical strain ε and has to be maximized to increase the sensitivity of the sensor to deformation [1].

$$GF = \frac{1}{R}\frac{dR}{d\varepsilon} \tag{2.8}$$

The piezosensitivity is defined as the fractional change in electrical resistance corresponding to a variation of the applied pressure and is the fundamental parameter for any kind of pressure sensor [2]:

$$S_p = \frac{dR}{R}\frac{1}{dP} = \frac{d\ln R}{dP} \tag{2.9}$$

2.1 Piezoresistive conductor-insulator composites

Piezoresistive composites have generated a large interest in both the scientific community and industrial research because of their unique electrical and mechanical properties e.g. force and strain sensors [3, 4], pressure sensors [5] and tactile sensors [6, 7].

The piezoresistive activity of composite materials can show two opposite behaviours: on the one hand literature reported on composite materials that suffer a decrease of electrical resistance by increasing the applied external pressure, namely negative pressure coefficient of resistance (*NPCR*) effect [8, 9, 10] . On the other hand several authors showed the reverse behaviour, i.e. positive pressure coefficient of resistance (*PPCR*) effect, where the electrical resistance rises upon increasing the external load [11, 3]. In general, the electrical conduction of these composites is described by the percolation theory, where the sudden insulator-conductor transition, defined as 'percolation threshold', is achieved in correspondence of a small variation of the conductive filler fraction.

Composite materials showing the *PPCR* effect usually are characterized by a low percolation threshold and are based on conductive filler having a high aspect ratio, such as fibers and nanotubes. As a consequence, by applying an external pressure, the relative resistance increases upon the sample compression due to the destruction of the existing conductive network [12].

Among the *NPCR* group, that is the more interesting and studied family, it is possible to distinguish mainly two theories explaining the electrical conduction mechanism: (i) the percolation theory, as in the *PPCR* case, and (ii) the tunnelling conduction mechanism.

2.1.1 Percolation conduction mechanism

This theory describes the material behaviour below the percolation threshold as electrical insulator. Then upon increasing the amount of conductive filler, the resistivity suddenly prompt drops [13, 14]. In these composites, by increasing the amount of conductive filler, the gap between two neighboring particles decreases enough to bring them in contact, thus leading to the formation of local conductive path. If local conductive paths impenetrate the whole insulating matrix, an effective conductive path is formed, contributing to the bulk electrical conductivity of the material [15]. The same process takes place when the material is subjected to a compressive pressure as representatively sketched in Fig.2.1. At the beginning the particles are distant enough to guarantee an insulating behaviour, while when the

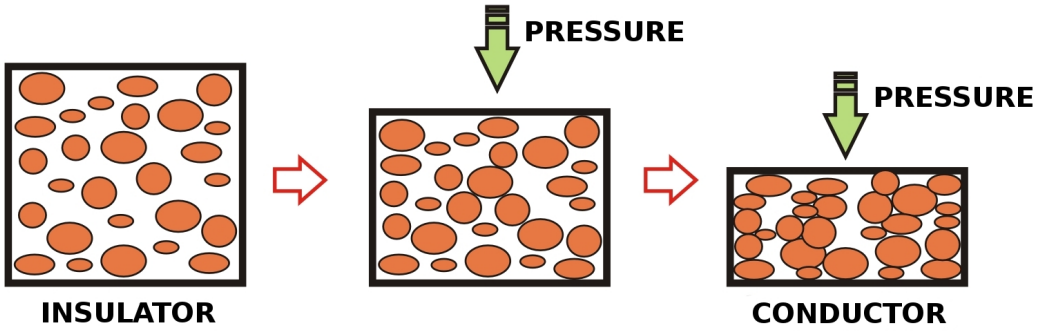

Figure 2.1. Sketch of the percolation conduction mechanism in insulator-conductor composite under uniaxial pressure.

matrix is deformed the particles come closer touching each other creating conductive paths that decrease the electrical resistance of the sample.

The percolation conduction mechanism can be simplified considering the insulating matrix as a porous medium and the electrical current as a liquid flowing through this medium. Then a mathematical model is used to describe the possibility of the liquid to pass through the porous matrix and reaching the base. The material is designed as a three dimensional matrix composed by points and connections that could be opened and closed, controlling the flowing of the fluid. Any connection has a probability p of being open, let the fluid flowing, and vice versa a *(1-p)* probability of being close. Considering the matrix as an infinite network, it has to be defined also a probability of the fluid to cross the whole material. This global probability has two limit conditions (0 corresponding to electric insulator behaviour and 1 to electric conductor) and is a function of the local probability. Therefore there is a critic probability p_c to switch the global probability of the system from 0 to 1 and returning to the electrical conduction, thus switching from insulator to conductor behaviour. Similarly is defined a critic concentration x_c around which there is a large conductivity variation with small concentration variation:

$$\sigma \propto (x - x_c)^t \tag{2.10}$$

where t is the critical exponent that determines the trend of the function around the critic concentration [16]. The same consideration can be done for the pressure defined as critic applied pressure.

2.1.2 Tunnelling conduction mechanism

As for the composite based on percolation conduction, in absence of external load the filler particles are separated from each other by the insulating matrix, thus the electrical resistance value of the material is extremely large (it is comparable to the matrix one). Each conductive particle is separated from the others by a thin insulator layer representing the tunnelling barrier [17]. When a mechanical deformation is induced, the insulating layer thickness between the conductive particles decreases and the fillers form a sequence of tunnelling pathways, resulting in a large reduction of the bulk electrical resistance, as sketched in Fig.2.2. It has been demonstrated that in these composites the shape and dimension of the filler particles become as important as the filler nature and amount [18]. In particular, the composites prepared with conductive particles presenting sharp and nanostructured tips on the surface exhibit a huge variation of the electrical conduction in response to a mechanical strain. In fact, this morphology is responsible for a local electric field enhancement [19] that considerably increases the tunnelling probability through the insulating barrier [9, 20]. Anyway tunnelling conduction is the dominant mechanism in these composites, but is not the only present. Electrical field induced emission [21], Richardson-Schottky transmission types and Pole-Frenkel conduction [22] are secondary order conduction mechanisms and therefore negligible. In contrast the percolation mechanism is negligible in the pressure range of interest for this study, while for elevate pressures it becomes predominant because the insulating layer cannot avoid anymore the contact between conductive particles strictly close to each other.

In the composites the total electrical resistance is a function of both the resistance through each conducting particle and the polymer matrix. Assuming that the resistance of the matrix is constant everywhere, the resistance of the paths perpendicular to the current flow may be neglected, and, thus, the number of conducting particles between electrodes becomes a factor in this relationship, as well as the number of conducting paths [10]. The total resistance can then be described as:

$$R = \frac{(L-1)\,R_m + L\,R_c}{S} \approx \frac{L\,(R_m + L\,R_c)}{S} \tag{2.11}$$

where R is the composite resistance, R_m the resistance between two adjacent particles, R_c the resistance across one particle, L the number of particles forming one conducting path, and S the number of conducting paths.

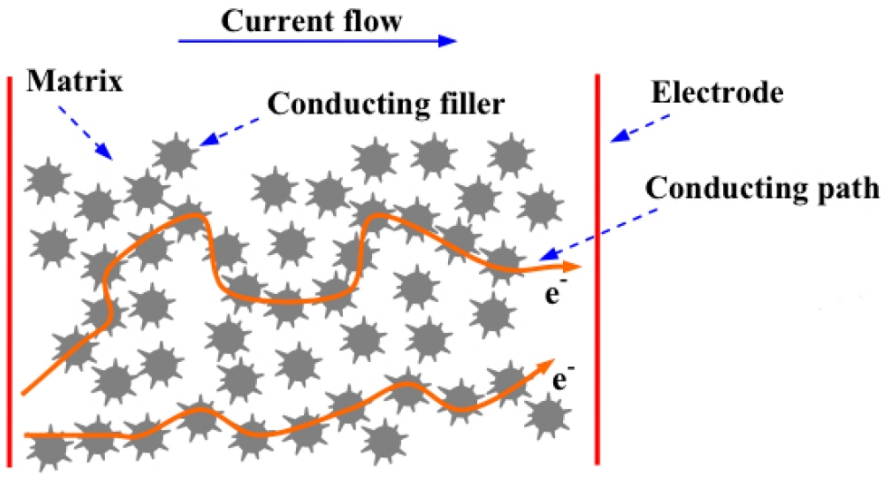

Figure 2.2. Sketch of the tunnelling conduction mechanism in insulator-conductor composite under uniaxial pressure.

Starting from this simple equation, the mathematical models described in the following sections were elaborated and proposed to describe the piezoresistive behaviour of the metal-polymer composites prepared in this thesis work.

2.1.2.1 Piezoresistivity under compressive pressure

Piezoresistive metal-polymer composites are soft and easily deformable materials, even if the content of metal particles is above 50% in volume. Therefore dimensions and shape of the samples suffer considerable changes under external forces. Under this assumption, the electrical resistivity that is an intensive physical quantity is not constant anymore throughout the whole sample and it results impossible to make an evaluation on it. Hence, in this thesis work, the mathematical models and the data are evaluated in terms of electrical resistance hence dependent on the dimension of the sample.

Many mathematical analyses of the piezoresistivity in conductor-filled polymer composites have been presented in literature. The models based on tunnelling conduction mechanism consider the tunnelling junction composed by two particles, separated by an insulating polymer layer, as basic unit. The computation is then extended to the whole sample, by considering the conductive paths across the material as constituted by chains of tunnelling junctions. In all these models the resistance across the particle is neglected because the

resistivity of the polymer is far more than the metal one. According to the analysis of Simmons [23], the tunnelling current between two adjacent particles at low applied voltage can be expressed as:

$$I = \frac{3a^2\sqrt{2m\varphi}}{2d}\left(\frac{e}{h}\right)^2 V exp\left(-4\pi d\sqrt{\frac{2m\varphi}{h^2}}\right) \tag{2.12}$$

where m and e are the electron mass and charge respectively, h the Plank's constant, V the applied voltage, d and j are the width and the height of the potential barrier between two adjacent particles and a^2 is the effective cross-sectional area where the tunnelling occurs.

From equation 2.12, Zhang et al. [10] obtained the resistance of a single barrier and then, considering the effect of all the tunnelling paths, the total resistance R of the composite sample:

$$R = \frac{L}{S}\left(\frac{4\pi hd}{3a^2\gamma e^2}\exp\left(2\gamma d\right)\right) \tag{2.13}$$

where L is the number of particles forming one tunnelling path, S is the total number of paths in a sample and

$$\gamma = 2\pi\sqrt{\frac{2m\varphi}{h^2}} \tag{2.14}$$

When a uniaxial compressive pressure is applied to the sample, its thickness is reduced as well as the average distance between adjacent particles. Then the value of resistance at a given applied pressure R_p can be calculated from the original resistance at zero stress R_0 as:

$$R = R_0\frac{d_p}{d_0}\exp\left(2\gamma\left(d_p - d_0\right)\right) \tag{2.15}$$

where d_p and d_0 are respectively the thickness of the interparticle insulating layer under pressure and at zero-stress. This variation in the gap is caused only by the deformation of the polymer since, comparing the compressive moduli, the metal particles result non-deformable with respect to the PDMS matrix. Therefore the insulating layer d_p can be calculated from the applied pressure p and the polymer compressive modulus G as:

$$d_p = d_0\left(1 - \varepsilon\right) = d_0\left(1 - \frac{p}{G}\right) \tag{2.16}$$

Then the equation for computing the electrical resistance of the sample under uniaxial pressure p can be found by substituting equation (2.16) in equation (2.15), thus obtaining:

$$R = R_0\left(1 - \frac{p}{G}\right)\exp\left(-2\gamma d_0\frac{p}{G}\right) \tag{2.17}$$

A more complex mathematical model was proposed by Lantada et al. [24] to explain the behaviour of QTC^{TM} (Quantum Tunnelling Composite by Peratech), but it can be applied to any metal-elastomeric polymer composite in which the conductive mechanism is based on quantum tunnelling effect. The behaviour of the material was modeled by adding to the quantum model of a potential barrier the influence of compressive forces, their time of application and temperature. Since the tunnelling current is linked to the probability of an electron to cross the insulating gap that corresponds to the square root of the barrier transmission coefficient, the electrical resistance of the composite is inversely proportional to this parameter. The value of resistance R, as a function of the physical perturbations, results proportional to the square root of the ratio of the barrier transmission coefficient in the initial state T_0 and the one under the applied boundary conditions of temperature, pressure and time of compression:

$$R\left(p,t,T\right) = R_0 \left(\frac{T_0}{T}\right)^{\frac{1}{2}}$$

$$T_0 = \left(1 + \frac{\varphi_0^2 \left(\sinh\left(\gamma_0 d_0\right)\right)^2}{4E\left(\varphi_0 - E\right)}\right)^{-1} \tag{2.18}$$

$$\gamma_0 = 2\pi\sqrt{\frac{2m\left(\varphi_0 - E\right)}{h^2}}$$

where d_0 and j_0 are the width and the height of the potential barrier in the initial state and E is the energy of the electrons.

They hypothesized that both the height and the width of the potential barrier are modified in the same way by changes in pressure and temperature. In order to quantify this variation, the viscoelastic behaviour of the elastomeric matrix was simulated by using Burger's model, while the effect of the temperature was considered as a linear thermal expansion term. Since in the present work the measurements were performed at room temperature and with a compression velocity high enough to neglect the creep effect of PDMS, the dependences on time and temperature in the variation of potential barrier dimensions were neglected. The formula obtained was equal to equation (2.16).

Therefore the expression of the electrical resistance under uniaxial compression can be

found combining equation (2.18) with equation (2.16):

$$R = R_0 \left(\frac{1 + \frac{\varphi^2 \left(\sinh\left(2\pi d \sqrt{2m(\varphi - E)/h^2} \right) \right)^2}{4E(\varphi - E)}}{1 + \frac{\varphi_0^2 \left(\sinh\left(2\pi d_0 \sqrt{2m(\varphi_0 - E)/h^2} \right) \right)^2}{4E(\varphi_0 - E)}} \right)^{\frac{1}{2}} \tag{2.19}$$

where:

$$\varphi = \varphi_0 \left(1 - \frac{p}{G} \right) \qquad d = d_0 \left(1 - \frac{p}{G} \right) \tag{2.20}$$

The thickness of the insulating layer between the particles was computed assuming all metal particles as spherical, with the same size and arranged in a cubic lattice [25]. The interparticle separation was estimated with this approximation, even if rough, because of the strong differences in dimension and shape of the particles. With this simplification d_0 can be expressed as:

$$d_0 = D \left(\left(\frac{\pi}{6\nu_f} \right)^{\frac{1}{3}} - 1 \right) \tag{2.21}$$

where D is the mean particle diameter and n_f is the filler volume concentration.

To increase the accuracy of the models, the mechanical effects on compression modulus were taken in account. The stiffness of the materials rose with the applied pressure, therefore the modulus cannot be considered constant. The value of G was estimated from the derivative of the experimental stress-strain curve and subsequently fitted as a function of the pressure. The final expression of the compression modulus was:

$$G = k_1 + k_2 p + k_3 p^2 \tag{2.22}$$

where k_1, k_2 and k_3 are fitting parameters.

2.1.2.2 Piezoresistivity under tensile pressure

The piezoresistive composite based on tunnelling conduction mechanism also shows huge variations of electrical resistance when subjected to tensile pressure. This behaviour is in contrast with the results obtained from resistance characterization as a function of compression. It was expected that stretching the material would lead to a thickening of the interparticle layers in the direction of the force, thus increasing the electrical resistance.

When considering the most common polymeric matrices i.e. silicone (PDMS), one can assume that the material is nearly or purely incompressible [26]. When stretched in one direction it contracts in the directions perpendicular to the applied load by keeping the volume constant. Then in the composite, the gaps between the particles in the plane perpendicular to the applied pressure are reduced proportionally with the applied tensile strain, resulting in an increasing of the tunnelling probability. The metal particles are randomly distributed along the material and are not perfectly aligned along planes, therefore a deformation in the direction perpendicular to the force would mean a redistribution of the particles in the composite that can create tunnelling paths along the samples. In this way, the resistance of the sample decreases exponentially with the applied pressure by following the tunnelling conduction mechanism.

A model starting from the assumption of total incompressibility of the composite material is proposed [27]. Therefore the variation of the insulator thickness between the particles, disposed on tunnelling paths, depends only on the deformation of the sample in the directions perpendicular to the applied pressure. In this case, the width of the potential barriers along the direction of the pressure (z) and on the perpendicular ones (x,y) can be expressed as:

$$d_z = d_0\ (1+\varepsilon) = d_0\ \left(1+\frac{p}{G}\right) \tag{2.23}$$

$$d_{x,y} = \frac{d_0}{\sqrt{1+\varepsilon}} = \frac{d_0}{\sqrt{1+\frac{p}{G}}} \tag{2.24}$$

where ε is the tensile strain, p the pressure and G the tensile modulus. Eq. (2.24) is valid assuming that the deformation along x and y is the same.

Combining equation (2.24) with equation (2.15) is then possible to obtain the variation of electrical resistance of the composite when subjected to tensile stress, considering the contribution of only one direction. The resulting equation has to be divided by a factor of 2, because the contributions along x and y (same magnitude) have to be considered like parallel resistances. Then R can be calculated as:

$$R = \frac{R_0}{2\sqrt{1+\frac{p}{G}}} \exp\left(-2\gamma \frac{\sqrt{1+\frac{p}{G}}-1}{\sqrt{1+\frac{p}{G}}}\right) \tag{2.25}$$

Bibliography

[1] M.K. Abyaneh and S.K. Kulkarni. Giant piezoresistive response in zinc-polydimethylsiloxane composites under uniaxial pressure. *J. Phys. D: Appl. Phys.*, 41:135405, 2008.

[2] F.G. Chang, F. Yang, S.X. Wang, N. Zhang, and G.L. Song. Enhanced piezoresistivity in Niâsilicone rubber composites. *Chinese physics B*, 18(2):652–657, 2009.

[3] G. Ausanio, A.C. Barone, C. Campana, V. Iannotti, C. Luponio, G.P. Pepe, and L. Lanotte. Giant resistivity change induced by strain in a composite of conducting particles in an elastomer matrix. *Sensors and Actuators A: Physical*, 127(1):56–62, 2006.

[4] G.M. Bayley, M. Hedenqvist, and P.E. Mallon. Large strain and toughness enhancement of poly(dimethyl siloxane) composite films filled with electrospun polyacrylonitrile-graft-poly(dimethyl siloxane) fibres and multi-walled carbon nanotubes. *Polymer*, 52(18):4061–4072, 2011.

[5] M.J. Jiang, Z.M. Dang, and H.P. Xu. Significant temperature and pressure sensitivities of electrical properties in chemically modified multiwall carbon nanotube/methylvinyl silicone rubber nanocomposites. *Applied Physics Letters*, 89(18):182902, 2006.

[6] G. Canavese, M. Lombardi, S. Stassi, and C. F. Pirri. Comprehensive characterization of large piezoresistive variation of Ni-PDMS composites. *Applied Mechanics and Materials*, 110-116:1336–1344, 2012.

[7] M. Shimojo, A. Namiki, M. Ishikawa, R. Makino, and K. Mabuchi. A tactile sensor sheet using pressure conductive rubber with electrical-wires stitched method. *IEEE Sensors Journal,*, 4(5):589–596, 2004.

[8] J.Y. Wu, C.X. Zhou, Q.W. Zhu, E.R. Li, G. Dai, L. Ba, Y.H. Huang, and J. Mei. Composite silicone rubber of high piezoresistance repeatability filled with nanoparticles. *Science in China, Series E: Technological Sciences*, 52(12):3497–3503, 2009.

[9] D. Bloor, K. Donnelly, P. J Hands, P. Laughlin, and D. Lussey. A metal-polymer composite with unusual properties. *J. Phys. D: Appl. Phys.*, 38:2851–2860, 2005.

[10] X.W. Zhang, P.Y. Zheng, and X.Q. Yi. Time dependence of piezoresistance for the conductor-filled polymer composites. *J Polym Sci Part B: Polym Phys*, 38(21):2739–2749, 2000.

[11] L. Chen, G.H. Chen, and L. Lu. Piezoresistive behavior study on finger-sensing silicone rubber/graphite nanosheet nanocomposites. *Advanced Functional Materials*, 17(6):898–904, 2007.

[12] J. Hwang, J. Jang, K. Hong, K.N. Kim, J.H. Han, K. Shin, and C.E. Park. Poly(3-hexylthiophene) wrapped carbon nanotube/poly(dimethylsiloxane) composites for use in finger-sensing piezoresistive pressure sensors. *Carbon*, 49(1):106–110, 2011.

[13] B. Lundberg and B. Sundqvist. Resistivity of a composite conducting polymer as a function of temperature, pressure, and environment: Applications as a pressure and gas concentration transducer. *Journal of Applied Physics*, 60(3):1074–1079, 1986.

[14] M. Hussain, Y.-H. Choa, and K. Niihara. Conductive rubber materials for pressure sensors. *Journal of Materials Science Letters*, 20:525–527, 2001.

[15] T. Ding, L. Wang, and P. Wang. Changes in electrical resistance of carbon-black-filled silicone rubber composite during compression. *Journal of Polymer Science Part B: Polymer Physics*, 45(19):2700–2706, 2007.

[16] D. Toker, D. Azulay, N. Shimoni, I. Balberg, and O. Millo. Tunneling and percolation in metal-insulator composite materials. *Physical Review B*, 68(4):041403, 2003.

[17] G.R. Ruschau, S. Yoshikawa, and R.E. Newnham. Resistivities of conductive composites. *Journal of Applied Physics*, 72(3):953–959, 1992.

[18] S. Stassi, G. Canavese, V. Cauda, S.L. Marasso, and C.F. Pirri. Evaluation of different conductive nanostructured particles as filler in smart piezoresistive composites. *Nanoscale Research Letters*, 7, 2012.

[19] C.J. Edgcombe and U. Valdrè. Microscopy and computational modelling to elucidate the enhancement factor for field electron emitters. *Journal of Microscopy*, 203:188–194, 2001.

[20] S. Stassi, G. Canavese, M. Lombardi, A. Guerriero, and C.F. Pirri. Giant piezoresistive variation of metal particles dispersed in PDMS matrix. *MRS Online Proceedings Library*, 1299, 2011.

[21] L.K.H. Beek and B.I.C.F. van Pul. Internal field emission in carbon black-loaded natural rubber vulcanizates. *Journal of Applied Polymer Science*, 6(24):651–655, 1962.

[22] R. Strumpler and J. Glatz-Reichenbach. Conducting polymer composites. *Journal of Electroceramics*, 3(4):329–346, 1999.

[23] J.G. Simmons. Electric tunnel effect between dissimilar electrodes separated by a thin insulating film. *Journal of Applied Physics*, 34(9):2581–2590, 1963.

[24] A.D. Lantada, P. Lafont, J.L.M. Sanz, J.M. Munoz-Guijosa, and J.E. Otero. Quantum tunnelling composites: Characterisation and modelling to promote their applications as sensors. *Sensors and Actuators A: Physical*, 164(1-2):46–57, 2010.

[25] S. Wu. Phase structure and adhesion in polymer blends: A criterion for rubber toughening. *Polymer*, 26(12):1855–1863, 1985.

[26] Y.S. Yu and Y.P. Zhao. Deformation of PDMS membrane and microcantilever by a water droplet: Comparison between Mooney-Rivlin and linear elastic constitutive models. *Journal of Colloid and Interface Science*, 332(2):467–476, 2009.

[27] S. Stassi, V. Cauda, G. Canavese, D. Manfredi, and C.F. Pirri. Synthesis and characterization of gold nanostars as filler of tunneling conductive polymer composites. *European Journal of Inorganic Chemistry*, 16:2669–2673, 2012.

Chapter 3

Spiky nanostructured nickel particles as filler of composites showing tunable electrical conductivity

This chapter presents a comprehensive investigation of the properties of a composite material based on conductive nickel filler in a silicone-insulating matrix. The mechanical, electrical, and thermal properties of the material are studied to explain the mechanism of conduction. In the absence of a deformation, the prepared composite shows no electric conductivity, even though the metal particle content is well above the expected percolation threshold. Upon samples deformation (compressive or tensile stress), the composite exploits a variation of electrical resistance up to nine orders of magnitude. This huge variation can be explained with the quantum tunnelling mechanism where the probability of an electron to tunnel from a particle to the next one is exponentially proportional to the thickness of the insulating layer between them and it is strongly enhanced by the morphology of the nickel particles, showing spiky nanostructured tips. Two different conduction theoretical models are proposed and compared with the experimental results.

The functional response of the material can be tuned varying the process parameters. Here, the effects of sample thickness, Nickel to PDMS ratio, PDMS Young's modulus and temperature on the piezoresistive behaviour of PDMS composites are fine evaluated.

Cost efficient materials, simplicity of the process, large sensibility, and harsh environment compatibility make this quantum tunnelling composite adapted to be integrated as sensing

coating for robotic applications.

3.1 Preparation of the composite

PDMS-Ni composites were prepared from nickel powder and bi-component polydimethylsiloxane (PDMS) supplied by Vale Inco (Type 123) and Dow Corning Corporation (SYLGARD 184), respectively.

The composite was prepared by dispersing the metallic powder in the PDMS copolymer at room temperature by gently mixing, in order to avoid the destruction of the tips on the surface of the particles. It has been demonstrated that a vigorous mixing destroys the nanometric tips on the surface of the particles, strongly decreasing the piezoresistive response of the final composite [1]. PDMS curing agent was then added to the blend. The obtained paste was then mixed manually again, poured in Poly(methyl methacrylate) (PMMA) hollow cavity shapes moulds, fabricated by milling technique, and outgassed under vacuum for 1 hour at room temperature. After all the air bubbles were removed, the mould was clamped between two PMMA plates in order to obtain flat surfaces. Then the composite was thermally cured at 75 °C for three hours. A graphical representation of the process flow is presented in Fig.3.1.

The composites were prepared by varying three parameters: the nickel filler to PDMS weight ratio (express in phr *per hundred resin*), the copolymer to curing agent ratio and the composite thickness. The combination obtained for all the samples are summarized in Tab.3.1.

Thickness	**PDMS copolymer-curing agent ratio**	
	3.33:1	**10:1**
1 mm	From 300 to 550 phr	From 250 to 550 phr
2 mm	From 300 to 550 phr	From 250 to 550 phr
3 mm	From 300 to 550 phr	From 250 to 550 phr

Table 3.1. Variation of process parameters for the preparation of PDMS-Ni composite samples

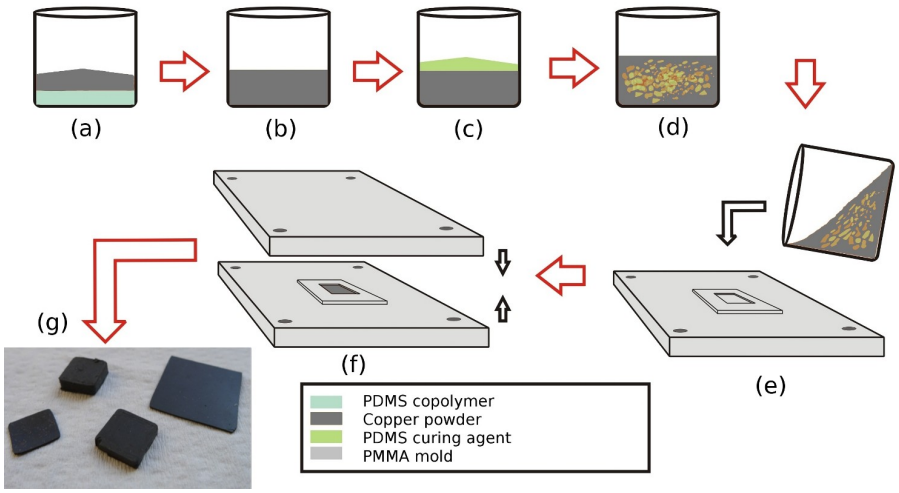

Figure 3.1. Process flow of the preparation of the composite material: (a) PDMS base weighing, (b) nickel particles weighing, mixing, (c) curing agent weighing, (d) mixing, mixture outgassing, (e) pouring in the mould, (f) closing with PMMA plates and (g) demoulding.

3.2 Characterization methods

The characterization techniques and instruments described below were used for all the composite materials presented in this thesis. Therefore their description was not repeated in the other chapters.

The morphological characterization of the PDMS-Ni composite was carried out by a field emission scanning electron microscope (FESEM, Zeiss SupraTM 40) with an accelerating voltage of 5 kV. Composite samples with a low content of metallic filler were previously cover by a nanometric layer of platinum (below 10 nm) in order to avoid charging effect on the polymer surface.

The viscoelastic properties of the materials were studied with a dynamic mechanical thermal analyzer (DMTA, Rheometric Scientific MKIII instrument), at a frequency of 1 Hz in the tensile configuration.

Functional analysis under compressive and tensile forces were performed with a universal mechanical testing machine (MTS Qtest 10) equipped with a load cell of 500 N, coupled with a Keithley 2635A sourcemeter connected to a home-made sample holder. The electrical resistance of the composite samples was evaluated with the four-point probe technique, by applying a constant voltage and measuring the current flowing through the material. During the functional characterizations, the metallic grips were carefully insulated from the samples.

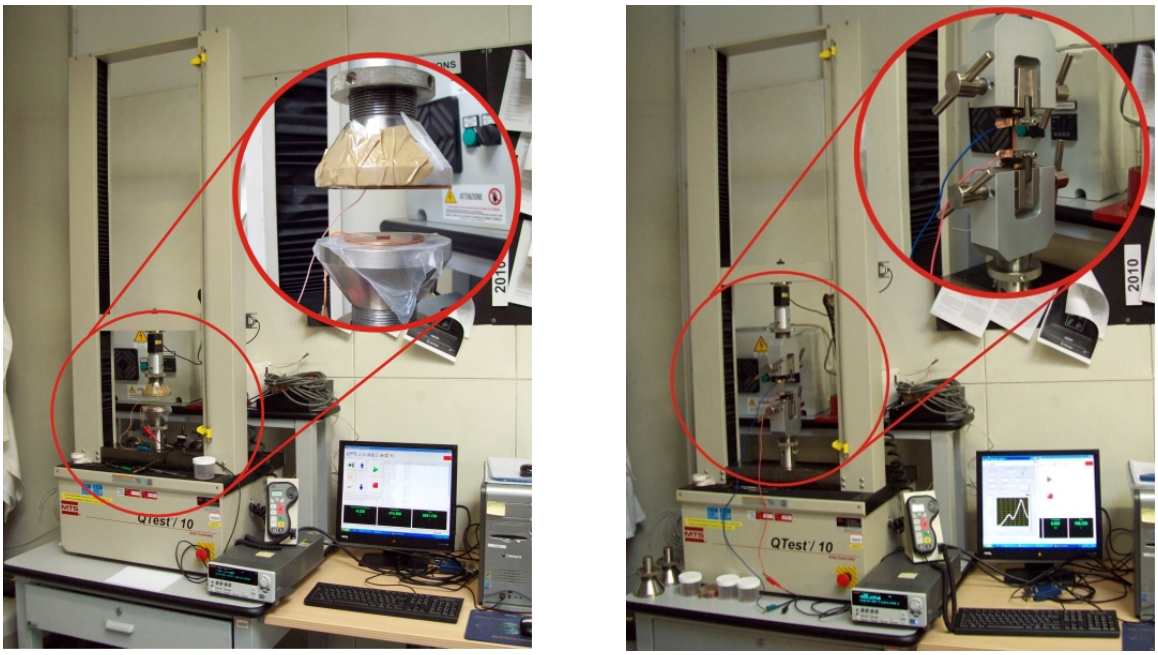

(a) (b)

Figure 3.2. Images of the experimental setup used for the functional characterization under uniaxial (a) compressive and (b) tensile pressures.

For the compression analysis, the samples were placed between two stiff copper plates, used as electrodes, and fixed to the grips of the test machine (Fig.3.2(a)). For the functional characterizations under tensile strain, strips of electrical conductive copper tape working as electrodes were clamped between each sample, in its undeformed state, and the universal test grips (Fig.3.2(b)). An automatically controlled heater has been placed around the sample holder for the functional characterizations above room temperature. All the operations and measurements performed by the whole apparatus were synchronized and collected with the use of a computer.

Current-voltage characteristics were carried out with a piezoelectric evaluation system (aixPES) supplied by aixACCT Systems. The samples were placed in a customized sample holder with the possibility of applying static uniaxial forces up to 5 kN. The sample holder included a resistance heater with the possibility of reaching temperatures up to 200 °C.

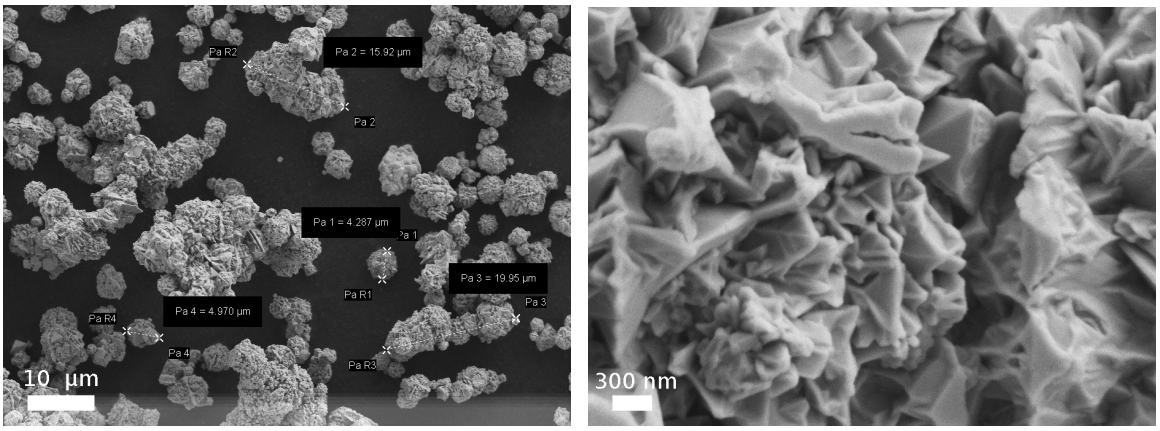

(a) (b)

Figure 3.3. FESEM images of nickel powder at different magnifications. The scale bars correspond to (a) 10 μm and (b) 300 nm

3.3 Structural and morphological analysis

The metallic powder and the piezoresistive composite samples were observed with FE-SEM to investigate the morphology of the nickel particles and their distribution inside the polymer matrix. The nickel particles have diameters in the range 3.5-7.0 μm (close to the 3.5-4.5 μm range quoted by the manufacturer) showing highly irregular surfaces with sharp tips (up to hundreds nanometers in length) and the tendency to create bigger aggregates, as shown in Fig.3.3. The mechanical mixing of the Ni powder with the polymer is able to break up the clusters and ensures a uniform dispersion of the particles in the polymeric matrix, without damaging their surface morphology. The images in Fig.3.4 show that the filler is well distributed through the insulating matrix and the polymer intimately coats the surface of the particles. This thin layer of PDMS placed between the particles prevents physical contact among them. Hence, no percolation paths are created throughout the sample, resulting in an insulating electrical behaviour in the uncompressed state. This phenomenon, previously observed by Bloor [1] and Abyaneh [2], takes place even if the volume percentage of filler is highly above the percolation threshold reported in other nickel [3] and different metal-polymer composite [4].

Under the effect of a compressive force the material suffers a deformation and the polymer barrier between each particle is reduced, proportionally with the applied load. The lowering of the insulating layer corresponds to an increase of the tunnelling probability,

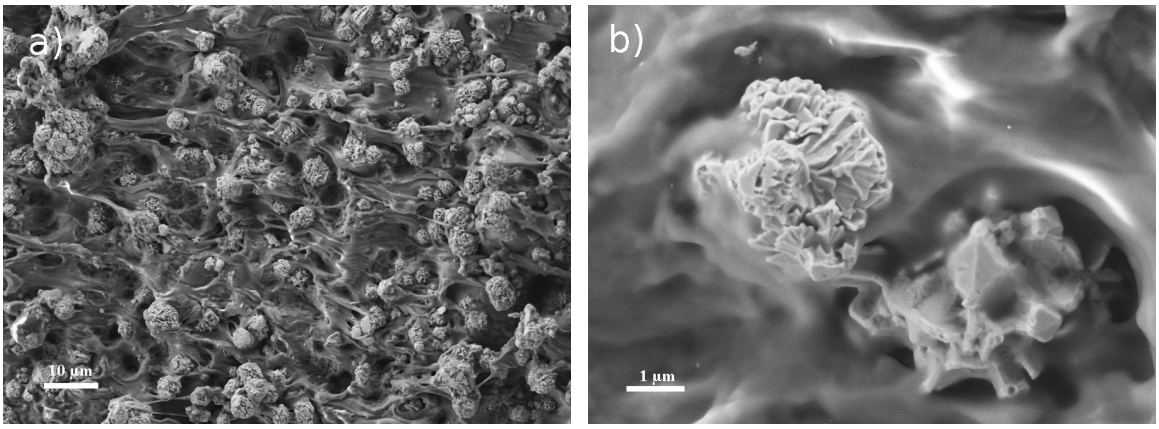

(a) (b)

Figure 3.4. FESEM images of PDMS-Ni composite at different magnifications. The scale bars correspond to (a) 10 and (b) 1 μm

therefore a decrease of the electrical resistance of the sample. Moreover, the charges accumulated on the nickel particles tips generate very large electric local fields. The presence of sharp protuberances has a key role in the conduction mechanism of the piezoresistive composite [1] since these geometries can favor the tunnelling phenomena with a very high field enhancement factor on the tip (up to 1000) [5] and consequently increases the variation of the composite resistance.

3.4 Functional characterization under compressive pressure

PDMS-Ni composite is a soft and easily deformable material, even if the content of metal particles is as high as 550 phr. Therefore, dimensions and shape of the samples suffer considerable changes under external forces. Under this assumption, the electrical resistivity that is an intensive physical quantity is not constant anymore throughout the sample, and it becomes impossible to make an evaluation on it. Hence, as previously explained in the theoretical chapter, all the data are evaluated in terms of electrical resistance that is dependent on the dimension of the sample.

The piezoresistive behaviour of the composite was evaluated as function of the weight content of nickel filler respect to the polymer matrix, of the PDMS copolymer-curing agent

weight ratio and of the thickness of the prepared samples. The footprint of the samples used for these characterizations was 10x10 mm^2

Fig.3.5 shows the dependence on the metallic filler content of the piezoresistive response of composite with a constant thickness of 3 mm. The graphs compare two different families of composites, one prepared with a PDMS copolymer-curing agent weight ratio of 3.33:1 and one with a ratio of 10:1. In the first one, the nickel content varies from 300 up to 550 phr, while in the latter from 250 up to 550 phr. Higher metal contents were difficult to process, since they inhibit the reticulating process and lead to stiff and fragile samples. The applied pressure was varied in the range between zero and 1.5 MPa.

All the composite samples have a value of resistance above 20 MΩ when uncompressed, confirming that most of the nickel particles are completely covered by an insulating layer of polymer and there are no conductive paths inside the composite, as observed during FESEM investigation (Fig.3.4). It can be noticed that there are minimum levels of nickel content below which there is no piezoresistive behaviour, corresponding to 300 phr (3.33:1) and 250 phr (10:1) composites.

By increasing the quantity of nickel, the composite becomes more sensitive to compression, starting to conduct at lower applied pressure. Moreover, the changing from the insulating condition to the maximum conductivity increases considerably up to reach the maximum variation of resistance, registered for the 550 phr samples with a variation of more than nine orders of magnitude over the whole range of applied uniaxial pressure.

The amount of nickel is not the only parameter which can be tuned to increase the composite sensitivity. By comparing the two graphs it results that the family with 10:1 PDMS matrix has a higher pressure sensitivity with respect to the 3.33:1 one. In fact the pressure sensitivity of these PDMS composites depends on the mechanical properties of the samples. A lower quantity of PDMS curing agent implies the production of a softer composite [6], allowing a higher deformation for a given load with a large relative displacement of the conductive filler and therefore a more enhanced decrease of the insulating barrier between the spiky particles.

This behaviour is analyzed in Fig.3.6 that shows the dependence of the variation of electrical resistance as function of the PDMS copolymer-curing agent ratio for quite all the nickel content compositions. As already stated the change in resistance is more pronounced for the composites with a lower content of curing agent (that has a lower Young's modulus

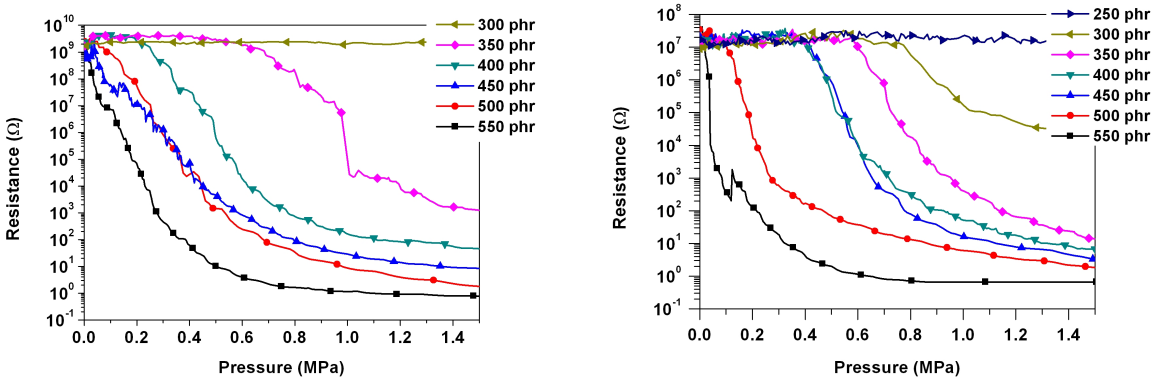

Figure 3.5. Piezoresistive response under compressive pressures as a function of metallic filler content of PDMS-Ni composites prepared with a PDMS copolymer-curing agent weight ratio of (a) 3.33:1 and (b)10:1.

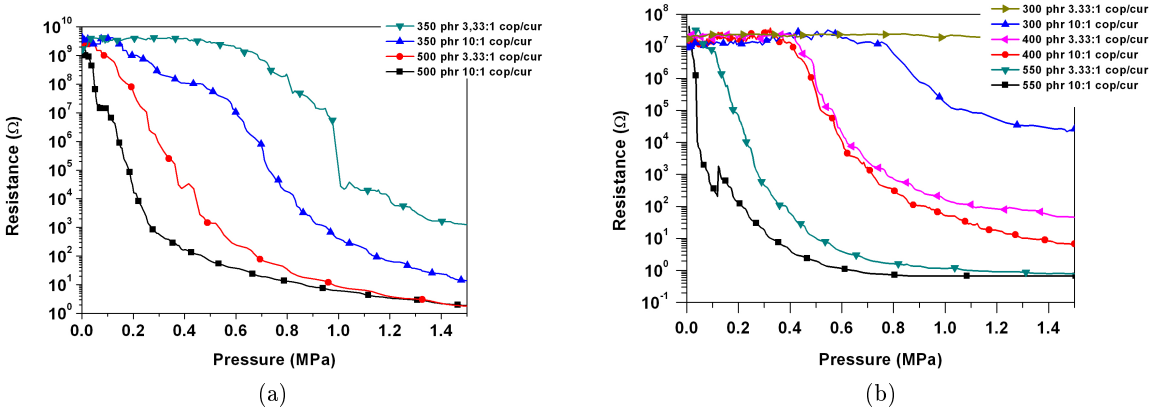

Figure 3.6. Piezoresistive response under compressive pressures of PDMS-Ni composites as a function of PDMS copolymer-curing agent weight ratio and metallic filler content.

[6]) and, moreover, this effect is more enhanced at lower metallic content due to the presence of larger amount of soft polymer between the particles. Indeed all samples with a 10:1 PDMS composition start to conduct at a lower compressive loading compared to the 3.33:1 samples and reach a lower resistance value at the maximum compression.

In order to establish the suitable thickness that could be used in tactile sensors, the piezoresistive response was evaluated for samples with thickness of 1, 2 and 3 mm. The measured data from composite with 10:1 PDMS copolymer-curing agent weight ratio and

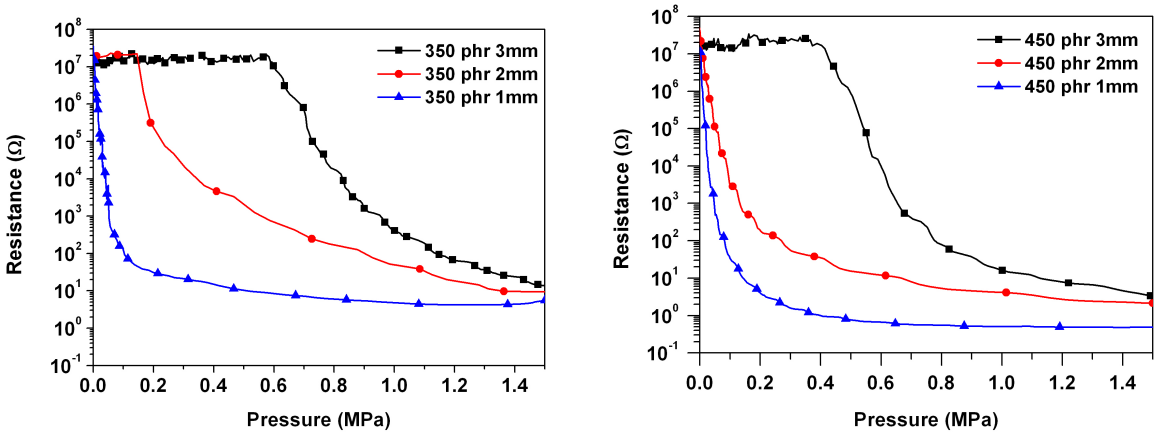

Figure 3.7. Piezoresistive response under compressive pressures of PDMS-Ni composites as a function of sample thickness.

nickel content of 350 phr and 450 phr are reported in Fig.3.7. As expected, thinner samples have an higher pressure sensitivity. The piezoresistive response as function of the thickness is not linear, as would be expected from the second Ohm's law, but more pronounced and irregular because the deformation of the samples is strongly dependent on the initial condition of shape, dimension and composition. This underlines that physical quantities like electrical resistivity or electric field are not constant through all the samples and explains why all the data in this work are reported in terms of electrical resistance.

In order to better understand the sensitivity of the material to applied uniaxial pressure, piezoresistive analysis as function of the rate of applied compression to the samples was performed. As visible in Fig.3.8(a), there is a difference of more than 2 orders of magnitude in the final resistance from pressing at 0.1 mm/min respect to 3 mm/min. The response of PDMS-Ni material to a compressive stress is not instantaneous. Inside the polymeric matrix, creep phenomena occur during the compressive test, inducing a delay for the nickel particles to reach the best configuration for tunnel conduction.

The same effect could be seen testing the electrical drift. In Fig.3.8(b) the values of resistance obtained while compressing the composite sample up to a certain pressure and then keeping it constant for 300 s are reported. It can be seen that the resistance continues to slightly decrease for the first seconds, because the polymer is subjected to a stress relaxation, and then remains constant. Both the graphs in Figure 2 were obtained from a 2 mm